

# Human-Robot Collaborative Site Inspection under Resource Constraints

Hong Cai and Yasamin Mostofi

**Abstract**—This paper is on human-robot collaborative site inspection and target classification. We consider the realistic case that human visual performance is not perfect (depends on the sensory input quality), and that the robot has constraints in communication with human (e.g., limited chances for query, poor channel quality). The robot has limited onboard motion and communication energy, and operates in realistic channel environments, experiencing path loss, shadowing, and multipath. We then show how to co-optimize motion, sensing, and human queries. Given a probabilistic assessment of human visual performance and a probabilistic channel prediction, we pose the co-optimization as Multiple-Choice Multidimensional Knapsack Problems. We then propose a Linear Program-based efficient near-optimal solution, mathematically characterize the optimality gap, showing it to be very small, and mathematically characterize properties of the optimum solution. We then comprehensively validate the proposed approach with extensive real human data (from Amazon MTurk) and real channel data (from downtown San Francisco), confirming that the proposed approach significantly outperforms benchmark methodologies.

**Index Terms**—Human-robot collaboration, Co-optimization of motion, sensing, and communication, Surveillance systems, AI reasoning methods.

## I. INTRODUCTION

Recent years have seen great developments in robotics, in areas such as navigation, motion planning, vision, learning and group coordination [1]–[5]. However, while robots are capable of more complicated tasks, there still exist many tasks that robots simply cannot perform to a satisfactory level, when compared to humans. A complex visual task, such as object recognition under uncertainty, is one example of such tasks [6]. Thus, a properly-designed collaboration between humans and robots is indispensable to many robotic missions.

More recently, the research community has been looking into different aspects of human-robot collaboration, including human decision-making modeling [7], operator decision-support [8], cooperative manipulation [9], and human-robot trust [10]. More related to this work are those papers that focus on robots querying humans for help. For instance, Dias et al. study how robots can recover from difficult states by asking for help [11] and Rosenthal et al. study the case of a robot asking for help in an office setting [12]. Particularly, for visual inspection tasks, a number of papers propose human-machine interface designs that allow the vision algorithm to query the human in order to improve its performance [6], [13]–[16]. In these papers, human visual performance is assumed either perfect or independent of the difficulty/quality of the individual sensory/image input. Human visual performance, however, is not perfect, as has been heavily acknowledged in cognitive psychology [17]. In addition, human visual performance can vary drastically depending on the sensory/image input, as we

Hong Cai and Yasamin Mostofi are with the Department of Electrical and Computer Engineering, University of California, Santa Barbara, USA (email: {hcai, ymostofi}@ece.ucsb.edu). This work was supported in part by NSF RI award #1619376 and NSF CCSS award #1611254.

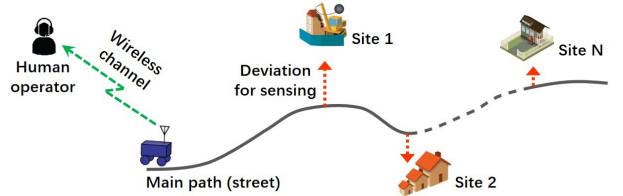


Fig. 1: The robot travels along a pre-defined path to inspect sites nearby. For each site, the robot decides how much it should deviate from the main path to move closer to the site for better sensing. It also needs to decide whether to ask the remote operator for help with target classification for this site. Human visual performance, however, is not perfect, and can vary depending on the sensing quality.

have established in our previous work [18], [19]. Then, in this paper, we are interested in human-robot collaboration when imperfect human performance is properly taken into account.

Next, consider robotic field operation and decision making under resource constraints, in terms of sensing [20]–[22], motion planning [23]–[25], and communication [26]–[28], which have received considerable attention over the years. More recently, researchers have become interested in communication-aware robotics, which considers realistic wireless channel environments and addresses the co-optimization of motion, sensing, and communication, under limited resources. For instance, Ghaffarkhah et al. study robotic target tracking and coverage under wireless fading channels [5], [29]. Yan et al. study the co-optimization of communication and motion in robotic operations [30]. Optimal control-based co-optimization methods have also been proposed in [31].

In this paper, we are interested in human-robot collaboration for site inspection under resource constraints, and while considering imperfect human performance and realistic communication channels. More specifically, we consider a realistic surveillance and patrolling scenario where there is a pre-defined path, near which there is a number of sites containing targets to be classified, as shown in Fig. 1. A robot is tasked with site inspection in this area. As the robot traverses this path and reaches a point close to a site, it has to decide whether (and to what extent) it should incur motion energy to deviate from the main path towards the site to sense it better, and whether it should ask for human help with this site. The robot then returns to the pre-defined path after a possible deviation. This scenario can capture several realistic cases of robotic missions. For example, a security surveillance drone can have a pre-defined patrol route, but may need to deviate from the route to investigate suspicious locations off the route. In another example, an indoor monitoring robot has to survey the offices down a hallway. The pre-defined route is then set along the hallway. When the robot needs to gather more sensing information about a room, it has to decide how far it should move into a room and whether it should query a remote human operator for help with this particular room.

The main goal of this paper is then to provide an optimization framework for a generic and realistic problem of human-

robot collaborative site inspection under resource constraints, which encompasses a number of real-world applications, as discussed. More specifically, in the considered setup of this paper, the robot's objective is to maximize its target classification performance at all the sites, under limited onboard energy constraints (including both communication and motion), with a limited access to a human operator to ask for help, and while considering the fact that human visual performance is not perfect. More specifically, we consider a realistic case that human visual performance is not perfect and varies depending on the sensory input, as we have established in [18], [19]. Thus, before deciding what to query the human operator, the robot needs to predict human visual performance over the sensory inputs. In [18], [19], we have shown how the robot can predict human visual performance using an a priori-trained machine learning pipeline. Furthermore, the robot has constraints in communication with the human operator. We consider two realistic communication constraints. In our first case, the robot is given a limited number of chances to query the human operator. This case realistically considers the impact of possible human work overload, which needs to be prevented by limiting the number of queries. Another cause of communication constraint is the quality of the wireless channel in the environment, when communicating with the human operator. In other words, the quality of the link may not be good enough to establish a reliable communication link all over the workspace, due to path loss, shadowing, and multipath fading in realistic channel environments. In our second case, the robot then needs to first predict the channel quality at unvisited locations in the environment. In our past work [32], we have shown how the robot can probabilistically predict the channel quality by utilizing a very small number of channel samples. These samples can be acquired from prior operations in the environment, collected online at the beginning of the operation, communicated to the robot by other robots, or acquired from the cloud. Based on this probabilistic wireless channel prediction, the robot then needs to decide where to communicate with the human operator, given a limited energy budget that can be used towards communication and motion.

Due to the communication restrictions and the imperfect human visual performance, the robot cannot query the operator all the time. Instead, the robot should only ask for help when human assistance can bring reasonable performance improvements (i.e., the task is doable by humans with a high probability) and when the cost of querying is reasonable. On the other hand, the robot may not have sufficient motion energy to sense the targets to the extent that it can fully rely on its own classification performance. Therefore, to achieve a good overall classification performance, it is necessary to co-optimize the robot's motion, sensing, and queries to the operator, while considering the impact of limited energy and the imperfect human performance, as is the goal of this paper.

**Statement of contributions:** In this paper, we show how to co-optimize motion, sensing, and human queries in human-robot collaborative site inspections, for the realistic case that the human visual performance is not perfect, and under limited energy resources and communication constraints to the operator, while considering realistic wireless channel environments

that experience path loss, shadowing, and multipath fading. Given probabilistic predictions of human performance and channel quality, we first show how to formulate the resulting co-optimization problems as Multiple-Choice Multidimensional Knapsack Problems (MMKP) [33]. We then propose a Linear Program (LP)-based efficient near-optimal solution to the NP-hard MMKP, and mathematically characterize the optimality gap, confirming that it can be considerably small. We also mathematically characterize properties of the optimal solution. Furthermore, we comprehensively validate our proposed approach with real human visual performance data that we acquired from extensive user studies on Amazon Mechanical Turk (MTurk), real wireless channel data collected from downtown San Francisco, and realistic motion and communication models. The numerical results show that our proposed approach properly co-optimizes motion, sensing, and queries, and significantly outperforms benchmark methodologies. Regarding our past conference paper in this area, in [18], we introduced the initial idea that imperfect human performance should be considered in human-robot collaboration, and characterized human visual performance based on MTurk data. This characterization is summarized in Sec. II, which will be used in our numerical results in Sec. IV and V. In [18], we further considered a simple scenario where the robot has to survey a number of sites but it has to go all the way to the site location if site inspection is needed, leaving no room for path optimization. Furthermore, imperfect communication links were not considered. In this paper, we consider a realistic setting where motion, sensing, communication, and human queries have to be co-optimized, under energy constraints, communication constraints, and while considering imperfect human performance. This results in a need for a new formulation and characterization, which we show how to achieve by using an MMKP-based approach.

The rest of the paper is organized as follows. In Sec. II, we summarize the system models to be used in the paper, including our previously-proposed probabilistic human performance characterization [18], [19], and the robot's motion energy model. In Sec. III, we give a brief overview of MMKP problems, which we shall use later in the paper. In Sec. IV and V, we show how to co-optimize the robot's motion, sensing, and queries to the operator, considering an imperfect human visual performance, under communication constraints to the operator, and given a limited energy budget. More specifically, in Sec. IV, the robot is given a limited number of queries to the operator, while in Sec. V, the quality of communication link to the remote operator may not be perfect everywhere in the workspace. The robot then has a limited energy budget that can be used towards communication or motion. Conclusions are given in Sec. VI.

## II. SYSTEM MODELING

In this section, we summarize our previous work on human and robot visual classification performance [18], and describe the robot's motion energy model to be used in the paper.

### A. Human and Robot Target Classification Performance

Consider the case where the robot has discovered a target via visual sensing (e.g., taking an image) and needs to classify

it based on a given set of target possibilities. For example, Fig. 2 (left) shows 4 possible targets shown to the robot prior to the task. The robot's sensing in the field is in general subject to noise, low resolution, occlusion, and other uncertainties, which will degrade its classification accuracy. Fig. 2 (right) shows a sample case where an image is corrupted by an additive Gaussian noise with a variance of 3. Based on MTurk studies, 74.4% of humans can still classify this lion correctly (see Fig. 4). If the robot could accurately model all the uncertainties and use the best classifier accordingly, it would outperform humans. However, this is impossible due to the complexity of a real-life visual task. This is why the robot can benefit tremendously from collaborating with the human by properly taking advantage of human visual abilities. In another example, Fig. 3 (left) shows a sample image that our ground robot took on our campus. In this image, the state-of-the-art vision algorithms fail to find the target (a person), while humans can easily find it, as shown in our previous work [19]. Human performance, however, is not perfect all the time, as we have established in [18], [19]. Fig. 3 (right), for instance, shows another campus image, where finding the target (a person) is difficult for most humans based on extensive MTurk user studies (several other hard cases have also been shown in [19]). Thus, it is important that the robot does not assume that the human operator is perfect and properly takes human performance into account when optimizing its collaboration.

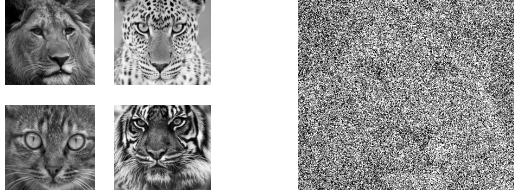


Fig. 2: (Left) Gray-scale images of lion, leopard, cat, and tiger used in our user studies [18]. (Right) A sample corrupted image (lion) with a noise variance of 3, which is shown to MTurk users in a user study to evaluate human visual performance as a function of noise.

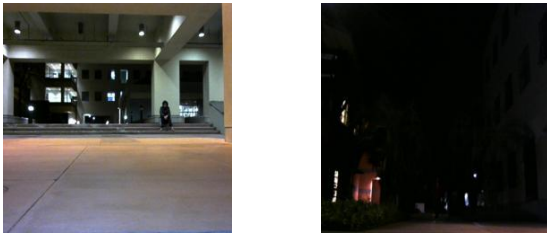


Fig. 3: Two sample campus images taken by a ground robot [19]. (Left) State-of-the-art vision algorithms fail to find the target (a person), while humans can easily find it. (Right) It is hard for humans to find the person in this image. For better viewing, see the color PDF.

#### B. User Studies to Acquire Real Human Data

In this paper, we are interested in the scenario where the fact that the human performance is not perfect is taken into account in the human-robot collaborative site surveillance. In this context, the robot then predicts human visual performance, and optimizes its field operation and human collaboration accordingly. Thus, acquiring real human data for validation purposes is considerably important.

In our previous work [18], human and robot performance curves were obtained for the following scenario. The robot

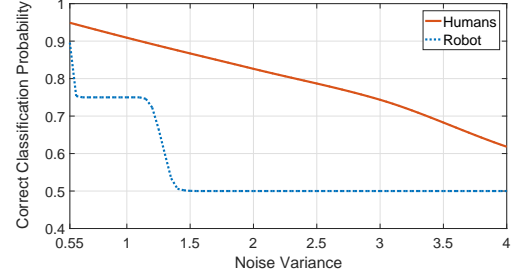


Fig. 4: Performance of human and robot in target classification of Fig. 2 (left). The human data is acquired from a human study with several Amazon MTurk users [18].

takes an image in the field, which is corrupted by an additive Gaussian noise with a known variance but an unknown mean, and then undergoes a pixel value clamping process unknown to the robot. The original image is chosen from the four images in the Fig. 2 (left). Then, a total of 160 noisy images were generated with different noise levels. We then conducted extensive user studies on Amazon MTurk, where, for each noisy image, several human users were asked to classify the target in the image to one of the four possibilities in Fig. 2 (left). Overall, 8000 human responses were collected, based on which the probability of human correct classification as a function of the noise level was obtained, as shown in Fig. 4. The figure further compares the human performance with that of the robot, and confirms that humans can achieve a much higher correct classification probability. For instance, for Fig. 2 (right), humans have an estimated correct classification probability of 0.744, which is considerably higher than that of the robot (0.5). However, as the figure also shows, human performance is not perfect, and can degrade significantly as the noise level increases. These performance curves will then be used for validation purposes in Sec. IV and V.

In this paper, our main focus is understanding the fundamentals of human-robot collaborative surveillance, when the human performance is not perfect and under resource constraints. We then test our proposed approach extensively with real human data where the main source of uncertainty is additive noise. We refer the readers to our past work [19], for a more comprehensive prediction of human visual performance, for any visual input with any source of uncertainty (not just additive noise), using machine learning. Such more advanced models of human performance can be integrated with the theoretical derivations of this paper as part of future work.

#### C. Motion Energy Model

In this section, we summarize the robot's motion energy model to be used in this paper. As shown by experimental studies, a mobile robot's motion power can be modeled by a linear function of its speed [23]:  $P_M = \kappa_1 u + \kappa_2$  when  $0 < u \leq u_{\max}$ , and  $P_M = 0$  when  $u = 0$ , where  $u$  and  $u_{\max}$  are the robot's speed and maximum speed, respectively.  $\kappa_1$  and  $\kappa_2$  are positive constants determined by the parameters of the motor, the external load, and the mechanical transmission system of the robot. Assuming that the robot travels at a constant speed  $u_{\text{const}}$ , the motion energy cost for a travel distance of  $x$  is then given by  $E_M = (\kappa_1 + \kappa_2/u_{\text{const}})x$ , which is a linear function of  $x$ . Thus, in our optimization formulations, the robot's motion energy cost is taken as a function of the traveled distance.

### III. MULTIPLE-CHOICE MULTIDIMENSIONAL KNAPSACK PROBLEMS

In this section, we briefly introduce the Multiple-Choice Multidimensional Knapsack Problem (MMKP) [33], which is a complex variant of the standard Knapsack Problem (KP).<sup>1</sup> In the subsequent sections, we then show how our resource-constrained human-robot collaborative site inspection problem can be posed as an MMKP.

In an MMKP, we are given  $C$  classes of items, where each class contains  $J_i$  items,  $\forall i \in \{1, \dots, C\}$ . It is assumed that there exist  $R$  types of resources and the respective budgets are given by  $b = [b_1, \dots, b_R]$ . In each class  $i$ , the  $j^{\text{th}}$  item is characterized by a non-negative reward  $p_{i,j} > 0$  and a non-negative weight vector  $W_{i,j} = [w_{i,j}^1, \dots, w_{i,j}^R] \succeq 0$ . The weight  $w_{i,j}^r$  denotes the needed resources from the  $r^{\text{th}}$  resource if the  $j^{\text{th}}$  item in class  $i$  is selected, for  $r \in \{1, \dots, R\}$ . The objective of the MMKP is then to pick *exactly* one item from each class such that the total reward is maximized, while satisfying all the  $R$  resource constraints. The standard MMKP can be formally stated as:

$$\begin{aligned} \max_z \quad & \sum_{i=1}^C \sum_{j=1}^{J_i} p_{i,j} z_{i,j} \\ \text{s.t.} \quad & \sum_{j=1}^{J_i} z_{i,j} = 1, \quad \forall i \in \{1, \dots, C\}, \\ & \sum_{i=1}^C \sum_{j=1}^{J_i} w_{i,j}^k z_{i,j} \leq b_k, \quad \forall k \in \{1, \dots, R\}, \\ & z_{i,j} \in \{0, 1\}, \quad \forall i \in \{1, \dots, C\} \text{ and } j \in \{1, \dots, J_i\}, \end{aligned} \quad (1)$$

where  $z = [z_{1,1}, \dots, z_{1,J_1}, \dots, z_{i,j}, \dots, z_{C,1}, \dots, z_{C,J_C}]$ , for  $i \in \{1, \dots, C\}$  and  $j \in \{1, \dots, J_i\}$ ,  $z_{i,j} = 1$  indicates that item  $j$  of class  $i$  is selected and  $z_{i,j} = 0$  indicates otherwise.  $z$  is then the stacked vector with all the decision variables for all the sites. When there is only one resource constraint ( $R = 1$ ), this special case is referred to as the Multiple-Choice Knapsack Problem (MCKP) [35]. MMKP is then the more general case where choosing an item can cost a number of different resources.

MMKPs have found many uses in practical applications related to resource management, e.g., adaptive multimedia systems [36] and cellular network management [37], as well as in robotic applications [38]–[42]. However, they are typically solved either by using integer program solvers, which can be computationally expensive for large problems, or by heuristics that have no theoretical optimality guarantees.

In this paper, we consider two human-robot collaborative settings where the robot experiences two different kinds of communication constraints. We show in Sec. IV and V how our problems can be formulated as MMKP and MCKP, respectively. As MMKP and MCKP are NP-hard combinatorial problems, we further show how to efficiently obtain near-optimal solutions based on LP relaxation, derive the optimality gap, and prove several properties of the optimal solution.

### IV. OPTIMIZING HUMAN-ROBOT COLLABORATION UNDER TOTAL QUERY CONSTRAINTS

In this section, we consider the case that the robot has been given a limited number of queries for human help during its

operation. As discussed earlier, this represents many realistic situations where the operator has to work with a number of robots and can thus not be overloaded with too many queries. The robot then has to optimally choose the sites for which humans have a high chance of accomplishing the visual task to query the operator. Furthermore, it has to co-plan its trajectory for site inspection, by considering its motion energy budget, its query budget, and human visual performance. In this section, we show how the robot can optimally achieve this.

#### A. Problem Setup

Consider the case where a robot travels along a pre-defined main path and has a total number of  $N$  sites to inspect, as shown in Fig. 1. In order to achieve a good target classification performance, the robot has to decide how far it should deviate from the pre-defined path to sense each site (it returns to the main path after each deviation), and whether it should ask for human help for each site. The robot is allowed to query the human  $M$  times during this operation and has a motion energy budget  $\mathcal{E}$  for the deviations, which is in addition to the motion energy required to travel the main path. We assume that the distance of each site to the pre-defined path is known such that motion energy costs can be estimated.

Let  $x_i \in [0, d_i]$  denote the deviation distance from the path to site  $i$ ,  $\forall i \in \{1, \dots, N\}$ , where  $d_i$  is the distance between the path and site  $i$ .  $\mathcal{E}_{M,i}(x_i)$  denotes the motion energy cost of a deviation of  $x_i$ , which includes both moving to the site and returning to the main path. Based on the sensing quality after traveling  $x_i$ , the correct classification probabilities of site  $i$  are  $p_{r,i}(x_i)$  and  $p_{h,i}(x_i)$  for the robot and the human, respectively.

In order to maximize the *average correct classification probability* of the sites, we have the following optimization problem:

$$\begin{aligned} \max_{\tilde{\gamma}, x} \quad & \frac{1}{N} \sum_{i=1}^N \tilde{\gamma}_i p_{h,i}(x_i) + (1 - \tilde{\gamma}_i) p_{r,i}(x_i) \\ \text{s.t.} \quad & \sum_{i=1}^N \mathcal{E}_{M,i}(x_i) \leq \mathcal{E}, \quad \sum_{i=1}^N \tilde{\gamma}_i \leq M, \\ & \tilde{\gamma} \in \{0, 1\}^N, \quad x \succeq \mathbf{0}, \end{aligned} \quad (2)$$

where  $\tilde{\gamma} = [\tilde{\gamma}_1, \dots, \tilde{\gamma}_N]^T$ ,  $x = [x_1, \dots, x_N]^T$ .  $\tilde{\gamma}_i = 1$  indicates that the robot should query the human for site  $i$  and  $\tilde{\gamma}_i = 0$  denotes otherwise, and  $\mathbf{0}$  is a vector of all 0s.

This optimization problem, however, is in general a non-convex Mixed Integer Nonlinear Program, solving which is computationally expensive [43]. We then show that by discretizing the motion decision space, this problem can be formulated as a Multiple-Choice Multidimensional Knapsack Problem (MMKP), which can be further closely approximated by solving a Linear Program (LP).

#### B. MMKP Formulation via Motion Space Discretization

In this section, we restrict the robot's deviation to quantized steps, which limits the robot's motion decision to a finite set. Let  $X_i = \{x_{i,j} : j \in \{1, \dots, D_i\}\}$  denote the set of possible motion steps for site  $i$ , where  $x_{i,j}$  represents a deviation distance corresponding to the  $j^{\text{th}}$  step and  $D_i$  is the number of possible steps for site  $i$ . The overall decision set for site  $i$  then becomes  $X_i \times \{0, 1\}$ , where  $\{0, 1\}$  is the decision set for whether the

<sup>1</sup>See [34] for a comprehensive overview of Knapsack problems.

robot should ask for human help for site  $i$ . This discretization then results in the following Integer Linear Program (ILP):

$$\begin{aligned} \max_{\gamma} \quad & \frac{1}{N} \sum_{i=1}^N \sum_{j=1}^{D_i} \gamma_{h,i,j} p_{h,i,j} + \gamma_{r,i,j} p_{r,i,j} \\ \text{s.t.} \quad (1) \quad & \sum_{j=1}^{D_i} \gamma_{h,i,j} + \gamma_{r,i,j} = 1, \quad \forall i \in \{1, \dots, N\}, \\ (2) \quad & \sum_{i=1}^N \sum_{j=1}^{D_i} (\gamma_{r,i,j} + \gamma_{h,i,j}) \mathcal{E}_{M,i,j} \leq \mathcal{E}, \\ (3) \quad & \sum_{i=1}^N \sum_{j=1}^{D_i} \gamma_{h,i,j} \leq M, \quad (4) \quad \gamma \in \{0, 1\}^{2 \times \sum_{i=1}^N D_i}, \end{aligned} \quad (3)$$

where  $\gamma$  is the stacked vector containing all the optimization variables as defined by Eq (4), with  $N$  denoting the number of sites and  $D_i$  representing the number of motion decisions of site  $i$ . More specifically, for site  $i$ , the set of decision variables is  $\{\gamma_{r,i,1}, \gamma_{h,i,1}, \dots, \gamma_{r,i,D_i}, \gamma_{h,i,D_i}\}$ , where  $\gamma_{r,i,j} = 1$  if the robot deviates  $x_{i,j}$  from the path and relies on itself for classification and  $\gamma_{r,i,j} = 0$  denotes otherwise. Similarly,  $\gamma_{h,i,j} = 1$  if the robot deviates  $x_{i,j}$  and queries the human *after* the further sensing and  $\gamma_{h,i,j} = 0$  denotes otherwise.  $\gamma$  is then the stacked vector of all the decision variables for all the sites. Note that due to constraint (3), for each site, only one variable will be equal to 1 and all the others will be 0 in a feasible solution. After the discretization, we represent  $p_{h,i}(x_{i,j})$ ,  $p_{r,i}(x_{i,j})$ , and  $\mathcal{E}_{M,i}(x_{i,j})$  by  $p_{h,i,j}$ ,  $p_{r,i,j}$ , and  $\mathcal{E}_{M,i,j}$  for conciseness, which are non-negative constants.

The next proposition shows that problem (3) is an MMKP by comparing its structure and parameters to those of a standard MMKP formulation.

**Proposition 1.** *Problem (3) is an MMKP, where there are  $N$  classes (sites) and for each class, there is a total number of  $2 \times D_i$  items (decisions). Furthermore, there are two resource constraints, which correspond to the motion energy budget and the query budget.*

*Proof.* This can be established by comparing problem (3) with problem (1).  $\square$

In the following proposition, we characterize the approximation error due to solving the discretized problem (3) instead of the original continuous problem (2).

**Proposition 2.** *Denote the optimums of problems (2) and (3) as  $f_{\text{Cont}}^*$  and  $f_{\text{MMKP}}^*$ , respectively. Then, we have  $f_{\text{Cont}}^* - f_{\text{MMKP}}^* \in [0, g]$ , where  $g = \max\{|p_{h,i,j+1} - p_{h,i,j}|, |p_{h,i,j+1} - p_{r,i,j}|, |p_{r,i,j+1} - p_{h,i,j}|, |p_{r,i,j+1} - p_{r,i,j}|\}$ ,  $\forall i \in \{1, \dots, N\}$  and  $j \in \{1, \dots, D_i\}$ .*

*Proof.* Since an optimal solution to problem (3) is also feasible to problem (2), we have  $f_{\text{Cont}}^* \geq f_{\text{MMKP}}^*$ . Suppose that for each site  $i$ , the motion cost  $\mathcal{E}_{M,i}(x_i)$  is non-decreasing in the deviation distance  $x_i$ . Denote an optimal solution to problem (2) by  $\tilde{\gamma}^*$  and  $x^*$ . For each site  $i$ , to obtain a feasible solution to problem (3), we replace  $x_i^*$  with  $x_{i,j}^* = \arg\min|x_{i,j} - x_i^*|$ , where  $x_{i,j} \leq x_i^*$ ,  $x_{i,j} \in X_i$ , and  $X_i$  is the discretized motion decision set for site  $i$ . Then, in the feasible solution to problem (3), for site  $i$ , the decision is represented by a deviation distance of  $x_{i,j}^*$  and a human query indicator  $\gamma_i^*$ . It can then be easily confirmed that the performance degradation is upper bounded by  $g$  for each site and thus, we have  $f_{\text{Cont}}^* - f_{\text{MMKP}}^* \leq g$ .  $\square$

Based on Prop. 2, it can be seen that if a fine-grained discretization is used, the difference between the optimums of problem (2) and problem (3) is negligible. However, a fine-grained discretization will introduce a large number of variables in the MMKP. Since an MMKP is an NP-hard combinatorial problem, it is not computationally efficient to solve a large-scale MMKP. Therefore, in the next section, we show how to efficiently obtain a solution based on LP relaxation and further prove that the LP-based solution is very close to the optimums of problems (2) and (3).

### C. Near-Optimal LP-based Solution

In this section, we propose an approach to efficiently obtain a near-optimal solution to problem (3) based on its LP relaxation.<sup>2</sup>

The LP relaxation is obtained by replacing the binary constraint  $\gamma \in \{0, 1\}^{2 \times \sum_{i=1}^N D_i}$  with a linear constraint  $\mathbf{0} \preceq \gamma \preceq \mathbf{1}$ , where “ $\preceq$ ” denotes a component-wise comparison, and  $\mathbf{0}$  and  $\mathbf{1}$  are vectors of all 0s and all 1s, respectively. We start this section by studying some properties of any feasible solution to this LP relaxation of problem (3). Based on these properties, we then characterize the number of fractional (non-binary) variables in an optimal solution to the LP relaxation of problem (3). We further prove that by properly rounding the LP optimal solution (to achieve a binary solution), we can achieve a solution that is very close to the optimum of problem (3), as well as problem (2). *To the best of our knowledge, this is the first proof characterizing the number of fractional variables in an optimal solution to the LP relaxation of an MMKP when there is more than one resource constraint.*

Consider an initial feasible solution to the LP relaxation of problem (3). We first describe a method to modify this solution to obtain another feasible solution. In other words, the variables in the modified solution still satisfy all the constraints of the LP. Suppose that in a feasible solution to the LP relaxation of problem (3), there is a number of fractional variables:  $\gamma_{h,i,j}$  with  $(i, j) \in S_H = \{(i, j) : \gamma_{h,i,j} \notin \{0, 1\}\}$  and  $\gamma_{r,k,m}$  with  $(k, m) \in S_R = \{(k, m) : \gamma_{r,k,m} \notin \{0, 1\}\}$ . We introduce some small changes to the fractional variables:

$$\hat{\gamma}_{h,i,j} = \gamma_{h,i,j} + \delta \alpha_{i,j} \quad \text{and} \quad \hat{\gamma}_{r,k,m} = \gamma_{r,k,m} + \delta \beta_{k,m}, \quad (5)$$

where  $|\delta| > 0$  is a small number, and  $\alpha_{i,j}, \beta_{k,m} \in \mathcal{R}$  are numbers to be determined. The symbol “ $\hat{\cdot}$ ” denotes the modified solution. The non-fractional variables stay the same.

Let  $\alpha$  denote a stacked vector of  $\alpha_{i,j}$  with  $(i, j) \in S_H$  and  $\beta$  denote a stacked vector of  $\beta_{k,m}$  with  $(k, m) \in S_R$ . In addition to requiring the modified solution to satisfy the optimization constraints of the LP, we also enforce that the modified solution uses the same amount of resources as the initial solution. Then,  $\alpha$  and  $\beta$  should satisfy the following system of linear equations:

$$\begin{aligned} (1) \quad & \sum_{(i,j) \in S_H} \alpha_{i,j} + \sum_{(i,m) \in S_R} \beta_{i,m} = 0, \quad \forall i \in S_f \\ (2) \quad & \sum_{(i,j) \in S_H} \alpha_{i,j} = 0, \\ (3) \quad & \sum_{(i,j) \in S_H} \mathcal{E}_{i,j} \alpha_{i,j} + \sum_{(k,m) \in S_R} \mathcal{E}_{k,m} \beta_{k,m} = 0, \end{aligned} \quad (6)$$

<sup>2</sup>Note that the LP relaxation of an ILP results in the same optimal solution as its Lagrangian relaxation [44].

$$\gamma = \underbrace{[\gamma_{r,1,1}, \gamma_{h,1,1}, \dots, \gamma_{r,1,D_1}, \gamma_{h,1,D_1}, \dots]}_{\text{variables for site 1}} \underbrace{[\gamma_{r,i,1}, \gamma_{h,i,1}, \dots, \gamma_{r,i,D_i}, \gamma_{h,i,D_i}, \dots]}_{\text{variables for site } i} \underbrace{[\gamma_{r,N,1}, \gamma_{h,N,1}, \dots, \gamma_{r,N,D_N}, \gamma_{h,N,D_N}]}_{\text{variables for site } N}^T \quad (4)$$

where  $S_f$  is the set of sites with fractional variables, line 1 corresponds to constraint (1) in problem (3) that the decision variables of each site should add up to 1, lines 2 and 3 ensure that the number of queries used and the motion energy usage do not change after modifying the initially-given feasible solution. It can be seen that if  $\alpha$  and  $\beta$  satisfy system (6), then constraints (1) - (3) of the LP relaxation of problem (3) are satisfied. Additionally,  $|\delta| > 0$  can be made sufficiently small such that  $\mathbf{0} \preceq \hat{\gamma} \preceq \mathbf{1}$ .

We can write system (6) in matrix form,  $A\psi = \mathbf{0}$ , where  $\psi = [\alpha, \beta]^T$  and  $A$  has the following form:

$$\left[ \begin{array}{cccc|cccc|c} \mathbf{1}_{\tilde{D}_{H,1}} & \mathbf{0}_{\tilde{D}_{H,2}} & \dots & \mathbf{0}_{\tilde{D}_{H,N}} & \mathbf{1}_{\tilde{D}_{R,1}} & \mathbf{0}_{\tilde{D}_{R,2}} & \dots & \mathbf{0}_{\tilde{D}_{R,N}} \\ \mathbf{0}_{\tilde{D}_{H,1}} & \mathbf{1}_{\tilde{D}_{H,2}} & \dots & \mathbf{0}_{\tilde{D}_{H,N}} & \mathbf{0}_{\tilde{D}_{R,1}} & \mathbf{1}_{\tilde{D}_{R,2}} & \dots & \mathbf{0}_{\tilde{D}_{R,N}} \\ \vdots & \vdots & \ddots & \vdots & \vdots & \vdots & \ddots & \vdots \\ \mathbf{0}_{\tilde{D}_{H,1}} & \mathbf{0}_{\tilde{D}_{H,2}} & \dots & \mathbf{1}_{\tilde{D}_{H,N}} & \mathbf{0}_{\tilde{D}_{R,1}} & \mathbf{0}_{\tilde{D}_{R,2}} & \dots & \mathbf{1}_{\tilde{D}_{R,N}} \\ \hline \mathbf{1}_{\tilde{D}_{H,1}} & \mathbf{1}_{\tilde{D}_{H,2}} & \dots & \mathbf{1}_{\tilde{D}_{H,N}} & \mathbf{0}_{\tilde{D}_{R,1}} & \mathbf{0}_{\tilde{D}_{R,2}} & \dots & \mathbf{0}_{\tilde{D}_{R,N}} \\ \mathcal{E}_{M,H} & & & & \mathcal{E}_{M,R} & & & \end{array} \right] \quad (7)$$

where  $\mathbf{1}_{\tilde{D}_{H,i}}$  and  $\mathbf{0}_{\tilde{D}_{H,i}}$  are  $1 \times \tilde{D}_{H,i}$  row vectors of all 1s and all 0s, respectively, and  $\mathbf{1}_{\tilde{D}_{R,i}}$  and  $\mathbf{0}_{\tilde{D}_{R,i}}$  are  $1 \times \tilde{D}_{R,i}$  row vectors of all 1s and all 0s, respectively,  $\forall i \in \{1, \dots, N\}$ .  $\tilde{D}_{H,i}$  and  $\tilde{D}_{R,i}$  are the numbers of fractional decision variables of site  $i$ , associated with the robot's decisions of querying the human and relying on its own classification, respectively.

The entries of  $A$  to the left of the vertical dashed line correspond to  $\alpha$  and those to the right correspond to  $\beta$ . The entries above the horizontal dashed line correspond to line 1 in system (6). The two bottom rows correspond to lines 2 and 3, respectively, where  $\mathcal{E}_{M,H} = [\mathcal{E}_{M,i,j}] \in \mathcal{R}^{1 \times |S_H|}$  is a row vector containing the motion energy costs of  $\gamma_{h,i,j}$  with  $(i, j) \in S_H$  and  $\mathcal{E}_{M,R} = [\mathcal{E}_{M,k,m}] \in \mathcal{R}^{1 \times |S_R|}$  is a row vector containing the motion energy costs of  $\gamma_{r,k,m}$  with  $(k, m) \in S_R$ .

If there exists a non-trivial solution to Eq. (6) and  $|\delta|$  is sufficiently small, then we can obtain another feasible solution by modifying the initial feasible solution based on Eq. (5). In order for Eq. (6) to have non-trivial solutions, matrix  $A$  needs to have a non-zero null space. In the following lemma, we formally characterize the conditions under which  $A$  has a non-zero null space.

**Lemma 1.** Consider a feasible solution to the LP relaxation of problem (3), and a modification of it to achieve another feasible solution through Eq. (5) and (6). There exist non-trivial solutions to system (6) (non-zero null space for matrix  $A$  in Eq. (7)) if any one of the following conditions hold:

- 1) the fractional variables are associated with more than 2 sites;
- 2) the fractional variables are associated with 2 sites and there are more than 2 fractional variables associated with at least one of the two sites;
- 3) the fractional variables are associated with 1 site and there are more than 3 fractional variables.

*Proof.* 1) It can be seen that there are  $n + 2$  rows in  $A$ , where

$n$  is the number of sites with fractional variables. Since the decision variables associated with each site add up to 1, there must be at least two fractional variables associated with each of these  $n$  sites. Thus, there are at least  $2n$  columns in  $A$ . Then, when  $n > 2$ , system (6) is under-determined, and therefore,  $A$  has a non-zero null space.

2) If the fractional variables are associated with exactly 2 sites and there are more than 2 fractional variables with at least one of the sites, then there will be 4 rows and more than 4 columns in  $A$ , resulting in a non-zero null space for  $A$ .

3) If the fractional variables are associated with 1 site and there are more than 3 fractional variables, then there will be 3 rows and more than 3 columns in  $A$ , resulting in a non-zero null space for matrix  $A$ .  $\square$

It is easy to confirm that there always exists a sufficiently small  $|\delta|$  such that  $\hat{\gamma}_{h,i,j}, \hat{\gamma}_{r,i,j} \in [0, 1]$ ,  $\forall i \in \{1, \dots, N\}$  and  $j \in \{1, \dots, D_i\}$ . Then, the existence of non-trivial solutions to system (6) and a sufficiently small  $|\delta|$  ensure that the modified variables satisfy the constraints of the LP. Denote the objective function values of the initial solution and the modified solution (based on Eq. (5) and (6)) by  $f_{LP}$  and  $\hat{f}_{LP}$ , respectively. Then,  $f_{LP}$  and  $\hat{f}_{LP}$  are related as follows:

$$\hat{f}_{LP} = f_{LP} + \delta\Delta, \quad (8)$$

where  $\Delta = \sum_{(i,j) \in S_H} \alpha_{i,j} p_{h,i,j} + \sum_{(k,m) \in S_R} \beta_{k,m} p_{r,k,m}$ . By applying Lemma (1) and analyzing  $\delta\Delta$ , we then characterize the fractional variables in an optimal solution to the LP relaxation of problem (3) in the following proposition.

**Proposition 3.** There exists an optimal solution,  $\gamma_{LP}^*$ , to the LP relaxation of problem (3) that satisfies the following:

- 1)  $\gamma_{LP}^*$  has at most four fractional (non-binary) variables;
- 2) The fractional variables are associated with at most two sites;
- 3) If the fractional variables are associated with two sites, then two fractional variables are associated with each site; if the fractional variables are associated with only one site, then there exists at most three fractional variables.
- 4) If  $\gamma_{LP}^*$  has no fractional variables, then the solution is also an optimal solution to the MMKP problem (3).

*Proof.* 1) Suppose that we have an optimal solution to the LP relaxation of problem (3) with fractional variables. If this optimal solution does not satisfy any of the conditions in Lemma 1, then there are at most four fractional variables. On the other hand, if the optimal variables satisfy any of the conditions in Lemma 1, then the fractional variables can be modified as described in Eq. (5), where  $\alpha$  and  $\beta$  are obtained from a non-trivial solution to system (6). With a small  $|\delta|$ , this modified solution satisfies the constraints of the LP. Denote the objective function values of the optimal LP solution and the modified feasible solution as  $f_{LP}^*$  and  $\hat{f}_{LP}$ , respectively. We then have  $\hat{f}_{LP} = f_{LP}^* + \delta\Delta$  based on Eq. (8). We discuss two cases based on the value of  $\Delta$ .

**Case 1** ( $\Delta = 0$ ): If  $\Delta = 0$ , then  $f_{LP}^* = \hat{f}_{LP}$ , regardless of the value of  $\delta$ . This indicates that there exist multiple optimal solutions to the LP and that if we modify the initial optimal

solution based on Eq. (5) and (6), we can obtain another solution which is also optimal. We can then increase  $|\delta|$  until at least one of the modified fractional variables becomes 0 or 1, resulting in a strictly smaller number of fractional variables in the solution. As long as the (modified) variables satisfy any one of the conditions in Lemma 1, this process can be repeated to reduce the number of fractional variables while maintaining the optimality of the solution. When we cannot perform this modification procedure anymore, we arrive at an optimal solution that does not satisfy any of the conditions in Lemma 1. Therefore, in this case, there exists an optimal solution  $\gamma_{LP}^*$  with at most four fractional variables.

**Case 2** ( $\Delta \neq 0$ ): If  $\Delta \neq 0$ , we can choose the sign of  $\delta$  such that  $\delta\Delta > 0$ , resulting in  $\hat{f}_{LP} > f_{LP}^*$ . This contradicts the assumption that  $f_{LP}^*$  is the optimum. Thus, in this case, the optimal solution can not satisfy any of the conditions in Lemma 1, and  $\gamma_{LP}^*$  have at most four fractional variables.

In summary, based on the analysis of the two cases above, there exists an optimal solution to the LP which does not satisfy any of the conditions in Lemma 1, and thus, has at most four fractional variables.

2) & 3) Based on part 1) of the proof, there exists an optimal LP solution that does not satisfy any of the conditions in Lemma 1. Such an optimal solution then also satisfies conditions (2) and (3) of this proposition.

4) As the LP relaxation of problem (3) has a larger feasible set, its optimum will be no worse than that of problem (3). If the optimal LP solution consists of only binary variables, then it is also an optimal solution to problem (3).  $\square$

Based on Prop. 3, the following theorem bounds the optimality gap between a feasible solution to problem (3) obtained by rounding the fractional variables (to  $\{0, 1\}$ ) in the optimal LP solution and the optimum of problem (3). Our derived bound is general and independent of the rounding technique.

**Theorem 1.** *Based on the optimal solution to the LP relaxation of problem (3), a feasible solution can be constructed to problem (3), which is less than or equal to  $2 \times (p_{max} - p_{min})/N$  from the optimum of problem (3), where  $p_{max} = \max\{p_{h,i}(x_i), p_{r,i}(x_i)\}$ ,  $p_{min} = \min\{p_{h,i}(x_i), p_{r,i}(x_i)\}$ ,  $\forall i \in \{1, \dots, N\}$  and  $x_i \in [0, d_i]$ .*

*Proof.* If the optimal LP solution has no fractional variables, then it is also optimal to problem (3). On the other hand, if it has fractional variables, Prop. 3 states that it has at most four fractional variables associated with at most two sites. Then, for sites with fractional variables, we round the fractional variables such that the overall query and motion energy constraints are still satisfied, which provides a feasible solution to problem (3). For the overall rounding of a site, the performance degradation is at most  $p_{max} - p_{min} = \max\{p_{h,i}(x_i), p_{r,i}(x_i)\} - \min\{p_{h,i}(x_i), p_{r,i}(x_i)\} \leq 1$ , where  $i \in \{1, \dots, N\}$  and  $x_i \in [0, d_i]$ , independent of the rounding method. Denote the optimums of the LP and the MMKP, and the objective function value of the LP-based solution obtained by rounding as  $f_{LP}^*$ ,  $f_{MMKP}^*$  and  $f_{LP-based}$ . We then have  $f_{LP}^* \geq f_{MMKP}^* \geq f_{LP-based}$ . Since there are at most two sites in the optimal LP solution that require rounding, we have

---

**Algorithm 1:** LP-based Solution to the MMKP Problem (3)

---

**CASE 1** ( $|S_f| = 0$ ): Set  $\gamma_{LP-based} = \gamma_{LP}^*$ .

**CASE 2** ( $|S_f| = 1$ ): Suppose that site  $i$  has fractional variables.

Set  $j_r^* = \operatorname{argmax}\{p_{r,i,j} : \mathcal{E}_{M,i,j} \leq \mathcal{E}_i\}$ .

Set  $j_h^* = \operatorname{argmax}\{p_{h,i,j} : \mathcal{E}_{M,i,j} \leq \mathcal{E}_i\}$ .

**if**  $M_f < 1$  **then**

| Set  $\gamma_{LP-based,r,i,j_r^*} = 1$ .

**else**

| If  $p_{r,i,j_r^*} \geq p_{h,i,j_h^*}$ , set  $\gamma_{LP-based,r,i,j_r^*} = 1$ . Otherwise, set  $\gamma_{LP-based,h,i,j_h^*} = 1$ .

**end**

Set the other variables associated with site  $i$  to 0. For the remaining sites, set the variables in  $\gamma_{LP-based}$  equal to their corresponding ones in  $\gamma_{LP}^*$ .

**CASE 3** ( $|S_f| = 2$ ): Suppose that sites  $i_1$  and  $i_2$  have fractional variables.

Set  $j_r^* = \operatorname{argmax}\{p_{r,i_1,j} : \mathcal{E}_{M,i_1,j} \leq \mathcal{E}_{i_1}\}$ .

Set  $j_h^* = \operatorname{argmax}\{p_{h,i_1,j} : \mathcal{E}_{M,i_1,j} \leq \mathcal{E}_{i_1}\}$ .

Set  $k_r^* = \operatorname{argmax}\{p_{r,i_2,j} : \mathcal{E}_{M,i_2,j} \leq \mathcal{E}_{i_2}\}$ .

Set  $k_h^* = \operatorname{argmax}\{p_{h,i_2,j} : \mathcal{E}_{M,i_2,j} \leq \mathcal{E}_{i_2}\}$ .

**if**  $M_f < 1$  **then**

| Set  $\gamma_{LP-based,r,i_1,j_r^*} = 1$  and  $\gamma_{LP-based,r,i_2,k_r^*} = 1$ .

**else if**  $M_f \geq 2$  **then**

| For site  $i_1$ , set the variable corresponding to the larger element of  $\{p_{r,i_1,j_r^*}, p_{h,i_1,j_h^*}\}$  to 1. For site  $i_2$ , set the variable corresponding to the larger element of  $\{p_{r,i_2,k_r^*}, p_{h,i_2,k_h^*}\}$  to 1.

**else**

| If  $p_{h,i_1,j_h^*} - p_{r,i_1,j_r^*} \geq p_{h,i_2,k_h^*} - p_{r,i_2,k_r^*} \geq 0$  **then**

| | Set  $\gamma_{LP-based,h,i_1,j_h^*} = 1$  and  $\gamma_{LP-based,r,i_2,k_r^*} = 1$ .

| **else if**  $p_{h,i_2,k_h^*} - p_{r,i_2,k_r^*} \geq p_{h,i_1,j_h^*} - p_{r,i_1,j_r^*} \geq 0$  **then**

| | Set  $\gamma_{LP-based,r,i_1,j_r^*} = 1$  and  $\gamma_{LP-based,h,i_2,k_h^*} = 1$ .

| **else**

| | For site  $i_1$ , set the variable corresponding to the larger one of  $\{p_{r,i_1,j_r^*}, p_{h,i_1,j_h^*}\}$  to 1. For site  $i_2$ , set the variable corresponding to the larger one of  $\{p_{r,i_2,k_r^*}, p_{h,i_2,k_h^*}\}$  to 1.

| **end**

**end**

Set the other variables associated with site  $i_1$  and  $i_2$  to 0. For the remaining sites, set the variables in  $\gamma_{LP-based}$  equal to their corresponding ones in  $\gamma_{LP}^*$ .

---

$f_{LP}^* - f_{LP-based} \leq 2 \times (p_{max} - p_{min})/N$ , which further gives  $f_{MMKP}^* - f_{LP-based} \leq 2 \times (p_{max} - p_{min})/N$ .  $\square$

Theorem 1 provides a general bound that applies to any form of rounding the fractional variables, while satisfying the resource constraints. Next, we present a specific method of rounding the fractional variables in Alg. 1 that optimizes the performance. For the rest of this section, we refer to this feasible solution to problem (3) given by Alg. 1 as the *LP-based solution*, which will be used in our numerical studies.

In Alg. 1, we denote  $\gamma_{LP}^*$  as the optimal solution to the LP relaxation of problem (3) and  $\gamma_{LP-based}$  as the LP-based feasible solution to problem (3) obtained via the rounding in Alg. 1. Similar to problem (3), subscripts “ $r, i, j$ ” (“ $h, i, j$ ”) indicate that the robot will deviate  $x_{i,j}$  towards the site, and then rely on its own classification (query the operator). In the optimal LP solution  $\gamma_{LP}^*$ ,  $S_f$  is the set of sites with fractional variables,  $M_f$  is the total number of queries allocated to the fractional variables:  $\sum_{i \in S_f} \sum_{j=1}^{D_i} \gamma_{LP,h,i,j}^*$ , and  $\mathcal{E}_i$  is the energy allocated to site  $i$ :  $\sum_{j=1}^{D_i} (\gamma_{LP,r,i,j}^* + \gamma_{LP,h,i,j}^*) \mathcal{E}_{M,i,j}$ .

Given the optimal LP solution, Alg. 1 optimizes the decisions over the sites with fractional variables,<sup>3</sup> such that the resulting solution contains only binary variables, and the energy consumption per site is kept the same as in the LP solution. For instance, in case 2, there is one site with fractional variables ( $|S_f| = 1$ ) in the LP solution (denoted as site  $i$ ). We then keep the same energy consumption of this site and solve for the best binary decision for site  $i$ , as follows. If the total number of queries allocated to the fractional variables is less than one ( $M_f < 1$ ), then we cannot query site  $i$ . In that case, we choose the position in site  $i$  with the best robot classification performance, subject to the motion energy consumption of site  $i$  ( $\mathcal{E}_i$ ), and set the corresponding variable to one. In this manner, the robot obtains an optimized binary decision for site  $i$ , using the same or less resource as allocated by the LP solution to site  $i$ . On the other hand, if  $M_f \geq 1$ , we first look at the two positions with the highest probabilities of human performance ( $p_{h,i,j_h^*}$ ) and robot performance ( $p_{r,i,j_r^*}$ ), respectively, given the energy consumption of this site. If  $p_{h,i,j_h^*} \geq p_{r,i,j_r^*}$ , then the robot should move to position  $j_h^*$  and ask about the site. Otherwise, the robot should move to position  $j_r^*$  and rely on itself. Similarly, in case 3, we solve for the best binary decisions for the sites with fractional variables, while ensuring that the motion energy consumption per site does not increase and the query budget is satisfied. Note that one cannot simply round the fractional variables to the closest integers, as this may violate the given resource constraints.

Next, we characterize the optimal gap between the LP-based solution to problem (3) and the optimum of the original continuous problem (2).

**Corollary 1.** *The LP-based solution to problem (3) is less than or equal to  $2 \times (p_{\max} - p_{\min})/N + g$  from the optimum of problem (2), where  $g$  is the approximation error bound introduced in Prop. 2.*

*Proof.* Based on Prop. 2 and Theorem 1, we have  $f_{\text{Cont}}^* - f_{\text{MMKP}}^* \leq g$  and  $f_{\text{MMKP}}^* - f_{\text{LP-based}} \leq 2 \times (p_{\max} - p_{\min})/N$ . Thus,  $f_{\text{Cont}}^* - f_{\text{LP-based}} \leq 2 \times (p_{\max} - p_{\min})/N + g$   $\square$

Although the LP relaxation-based solution does not always provide the exact optimal solution to problem (3), it offers a very close approximation. For instance, as Theorem 1 shows, the gap between the MMKP optimum and the LP-based feasible solution is very small, especially when  $N$  is large. Furthermore, unlike the NP-hard MMKP problem (3), solving the LP is computationally efficient. By choosing a fine-grained motion discretization, we can then get a near-optimal efficient solution to the original difficult continuous problem (2).

**Remark 1.** *(Optimality gap for general MMKPs) Our analysis can be extended to a general MMKP. More specifically, based on a similar analysis to that of Lemma 1 and Prop. 3, it can be confirmed that in an optimal solution to the LP relaxation of a general MMKP with  $R$  resource constraints, there exist at most  $2 \times R$  fractional variables and the fractional variables are associated with at most  $R$  classes. Based on similar arguments to those in Theorem 1, the optimality gap between the  $R$ -resource MMKP, whose objective function is the average*

<sup>3</sup>If a site has fractional variables, then all the variables of this site must be strictly less than 1 due to constraint (1) of Eq. (3).

reward from each class, and its LP-based solution is upper bounded by  $R \times (p_{\max} - p_{\min})/N$ , where  $p_{\max}$  and  $p_{\min}$  are the maximum and minimum rewards associated with a variable, respectively. We skip the proof due to the space limitation.

#### D. Properties of the Optimal Solution

Next, we study some properties of the optimal decisions.

**Proposition 4.** *In an optimal solution to problem (3), if  $\gamma_{h,i_1,j_1}^* = 1$  and  $\gamma_{r,i_2,j_2}^* = 1$ , where  $i_1, i_2 \in \{1, \dots, N\}$ ,  $j_1 \in \{1, \dots, D_{i_1}\}$ ,  $j_2 \in \{1, \dots, D_{i_2}\}$ , and  $\max\{x_{i_1,j_1}, x_{i_2,j_2}\} < \min\{d_{i_1}, d_{i_2}\}$ , then  $p_{h,i_1,j_1} - p_{r,i_1,j_1} \geq p_{h,i_2,j_2} - p_{r,i_2,j_2}$ .*

*Proof.* Suppose that in an optimal solution,  $\gamma_{h,i_1,j_1}^* = 1$ ,  $\gamma_{r,i_2,j_2}^* = 1$ , and  $p_{h,i_1,j_1} - p_{r,i_1,j_1} < p_{h,i_2,j_2} - p_{r,i_2,j_2}$ . By letting  $\gamma_{h,i_1,j_1} = 0$ ,  $\gamma_{r,i_1,j_1} = 1$ ,  $\gamma_{h,i_2,j_2} = 1$ , and  $\gamma_{r,i_2,j_2} = 0$ , we obtain a strictly better solution using the same amount of motion energy and the same number of queries, which is a contradiction.  $\square$

This proposition says that if we have two sites  $i_1$  and  $i_2$ , for which the robot will ask the human and rely on its own classification, respectively, then there should be a greater benefit from asking for human help for the first site.

**Proposition 5.** *In an optimal solution to problem (3), if  $\gamma_{r,i_1,j_1}^* = 1$  and  $\gamma_{r,i_2,j_2}^* = 1$ , where  $i_1, i_2 \in \{1, \dots, N\}$ ,  $j_1 \in \{1, \dots, D_{i_1}\}$ ,  $j_2 \in \{1, \dots, D_{i_2}\}$ , and  $\max\{x_{i_1,j_1}, x_{i_2,j_2}\} < \min\{d_{i_1}, d_{i_2}\}$ , then  $p_{r,i_1,j_1} - p_{r,i_1,j_2} \geq p_{r,i_2,j_1} - p_{r,i_2,j_2}$ .*

*Proof.* Suppose that in an optimal solution,  $\gamma_{r,i_1,j_1}^* = 1$ ,  $\gamma_{r,i_2,j_2}^* = 1$ , and  $p_{r,i_1,j_1} - p_{r,i_1,j_2} < p_{r,i_2,j_1} - p_{r,i_2,j_2}$ . Then by letting  $\gamma_{r,i_1,j_1} = 0$ ,  $\gamma_{r,i_1,j_2} = 1$ ,  $\gamma_{r,i_2,j_1} = 1$ , and  $\gamma_{r,i_2,j_2} = 0$ , we obtain a strictly better solution using the same amount of motion energy and the same number of queries, which is a contradiction.  $\square$

**Proposition 6.** *In an optimal solution to problem (3), if  $\gamma_{h,i_1,j_1}^* = 1$  and  $\gamma_{h,i_2,j_2}^* = 1$ , where  $i_1, i_2 \in \{1, \dots, N\}$ ,  $j_1 \in \{1, \dots, D_{i_1}\}$ ,  $j_2 \in \{1, \dots, D_{i_2}\}$ , and  $\max\{x_{i_1,j_1}, x_{i_2,j_2}\} < \min\{d_{i_1}, d_{i_2}\}$ , then  $p_{h,i_1,j_1} - p_{h,i_1,j_2} \geq p_{h,i_2,j_1} - p_{h,i_2,j_2}$ .*

*Proof.* The proof is similar to the proof of Prop. 5.  $\square$

Props. 5 and 6 state that if we have two sites  $i_1$  and  $i_2$ , at which the robot deviates two different distances,  $x_1$  and  $x_2$ , respectively, then the performance gain by moving from  $x_2$  to  $x_1$  at site  $i_1$  should be greater than that at site  $i_2$ .

#### E. Computation Time

In this section, we numerically compare the computational efficiency of solving the MMKP of problem (3) and obtaining its LP-based solution. In this comparison, there are 10 sites, 5 given queries, and the motion energy budget is 50% of what is needed to reach all the sites. The computations are performed on Matlab with an i7 CPU running at 3.4 GHz and the reported computation time is averaged over 500 problem instances.

Fig. 5 shows the computations of solving problem (3) and obtaining its LP-based solution w.r.t. the number of discretized motion steps per site. It can be seen that the LP-based solution is considerably more efficient. For instance, when a fine-grained discretization of 100 motion decisions per site is used, it takes an average of 268.23 s (or 4.47 min) to compute the MMKP solution. This makes it impractical to directly solve problem (3) in a robotics field operation. On the other hand, it takes an average of 0.0304 s to obtain the LP-based solution, making it a more favorable approach to efficiently compute a near-optimal solution in real-life applications where there can be many decision variables.

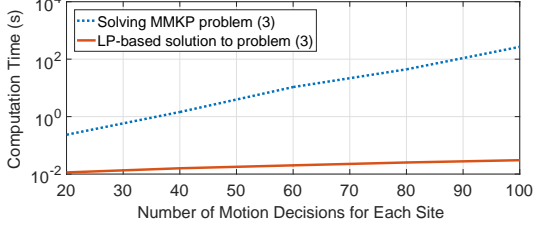


Fig. 5: Computation time of solving problem (3) and obtaining its LP-based solution for 10 sites w.r.t. the number of motion decisions for each site. The computation time is plotted in log scale.

#### F. Online Replanning to Cope with Operation Changes

As can be seen from Theorem 1 and Sec. IV-E, our proposed approach provides a computationally fast near-optimal solution to problem (3). Such computational efficiency enables the robot to quickly replan its actions to cope with possible changes in the operation. For instance, depending on the cognitive load of the human operator, the number of allowed queries may increase or decrease. During the operation, the set of sites which the robot is responsible for inspection may change as well, which also requires an efficient online replanning scheme. Given the updated command, the robot can then quickly recompute its future actions accordingly.

#### G. Simulation Results with Real Human Data

In this part, we numerically demonstrate the performance of our proposed collaboration framework for target classification under motion energy and query constraints, **using real human responses**. More specifically, we use the Amazon MTurk studies discussed in Sec. II, where we collected 8000 human visual responses over noisy images. The robot then uses Fig. 4 to assess human visual performance during its operation.

In the simulations, there are 10 sites, and the distance between each site and the path is 10 m. The noise variance is modeled as a quadratic function of the sensing distance:  $v = a_i d^2 + b_i$ , where  $a_i$  and  $b_i$  are parameters of the sensing model for site  $i$  [29]. We assume that the sites have three levels of sensing difficulty: easy, medium, and hard, encoded in  $a_i$ , which is then randomly assigned to the sites. Thus, given a sensing distance, the robot can easily assess the human's and its own performance as described in Sec. II. The motion model parameters are:  $\kappa_1 = 7.4$ ,  $\kappa_2 = 0.29$ , and the robot travels with a constant speed of 1 m/s. The motion parameters are based on real power measurements of a Pioneer 3DX robot [23]. The motion energy budget is taken as a percentage of the total energy required to visit all the site locations.

We consider a benchmark methodology where the collaboration is not fully optimized. More specifically, in the benchmark, the robot assumes a perfect human performance (which is a common assumption), but is aware of its own performance (blue dashed curve in Fig. 4). The robot then solves problem (3) with  $p_{h,i,j} = 1$ ,  $\forall i = \{1, \dots, N\}$ ,  $j \in \{1, \dots, D_i\}$ .

Next, we compare our proposed approach with the benchmark, by showing the resource savings from using our proposed approach, as compared to the benchmark. More specifically, given any combination of the motion budget and the query budget, we obtain the average correct classification probabilities of our proposed approach and the benchmark, by solving their respective optimization problems, and averaging

Ave. Correct Classification Prob.	Percentage Energy Saving
0.70	100%
0.75	39.39%
0.80	34.29%
0.85	35.29%
0.90 or higher	Inf

TABLE I: Motion energy saving by our proposed approach as compared to the benchmark. In this example, the robot is given 6 allowed queries.

Ave. Correct Classification Prob.	Percentage Query Saving
0.80	46.15%
0.85	55.62%
0.90 or higher	Inf

TABLE II: Saving of queries by our proposed approach as compared to the benchmark. In this example, the motion energy budget is 50% of what is needed to visit all the site locations.

over 100 problem instances with uniformly random sensing difficulty assignments over the sites. Based on these results, we can then see that to achieve the same average performance, our proposed approach would require smaller resource budgets, as compared to the benchmark.

More specifically, Table I shows the motion energy saving, enabled by our proposed approach, when the robot is given 6 allowed queries. It can be seen that our proposed approach requires considerably smaller energy budgets than the benchmark to achieve the same performance. For instance, when achieving an average correct classification probability of 0.75, our proposed approach requires a 39.39% smaller motion energy budget. In the table, “Inf” indicates that the benchmark method simply cannot achieve the performance no matter how much motion energy is given. Thus, our proposed approach is able to more efficiently utilize the given energy budget.

Table II summarizes the saving of queries by using our proposed approach, when the robot is given a motion energy budget of 50% of what is needed to reach all the site locations. It can be seen that our approach requires considerably less communication to the operator. For instance, to achieve an average classification accuracy of 0.85, our approach needs 55.62% fewer queries. This result shows that our proposed approach can reduce the overall burden on human operators who have to operate under fatigue and work overload.

## V. OPTIMIZING HUMAN-ROBOT COLLABORATION UNDER TOTAL ENERGY CONSTRAINTS

In the previous section, we considered the case where the communication bottleneck was human work overload, which limited the number of queries the robot could present to the remote operator. In this section, we consider another source of communication bottleneck, the cost of wireless transmission. More specifically, if the robot is operating in the areas where the communication link quality is not good everywhere, and/or if the robot has energy constraints on the communication side, then that can limit the number of successful queries to the human operator. In this section, we *explicitly* model and analyze this case, by considering the true energy cost of wireless transmissions in realistic communication environments that can experience path loss,

shadowing, and multipath fading. We further show how the robot can actively take the communication link quality into account when optimizing its collaboration with the operator. More specifically, we show that the resulting human-robot collaborative site survey problem, under both motion and communication energy constraints, can be posed as a Multiple Choice Knapsack Problem (MCKP) problem. We then derive an efficient near-optimal solution and mathematically characterize several properties of the optimal collaborative solution.

### A. Communication Energy Modeling and Prediction in Realistic Communication Environments

In this part, we summarize how to model the communication energy cost in realistic channel environments. Consider the case where the robot adopts the commonly-used MQAM modulation for transmission. As shown in the literature [45], the required transmission power is given by  $P_T = (2^{\log_2 M_c} - 1)\ln(5p_{b,\text{th}})/(-1.5\Upsilon)$ , where  $M_c$  is the modulation constellation size,  $p_{b,\text{th}}$  is the required Bit Error Rate (BER), and  $\Upsilon$  is the received Channel to Noise Ratio (CNR). Since real wireless channels experience path loss, shadowing and multipath fading, CNR has to be modeled stochastically and as a random process. As shown by [32], the CNR (in dB) at an unvisited location  $q$  can be best modeled by a Gaussian random variable, with the mean and variance given by

$$\begin{aligned}\bar{\Upsilon}_{\text{dB}}(q) &= H_q \hat{\theta} + \Psi^T(q) \Phi^{-1}(Y - H_Q \hat{\theta}), \\ \Sigma(q) &= \hat{\alpha}_{\text{dB}}^2 + \hat{\rho}_{\text{dB}}^2 - \Psi^T(q) \Phi^{-1} \Psi(q),\end{aligned}\quad (9)$$

where  $Y = [y_1, \dots, y_m]^T$  is the stacked vector of  $m$  a priori collected CNR measurements (in dB),  $Q = [q_1, \dots, q_m]$  contains the measurement locations,  $\hat{\theta}$ ,  $\hat{\alpha}_{\text{dB}}$ ,  $\hat{\beta}$ , and  $\hat{\rho}_{\text{dB}}$  are the estimated channel parameters,  $H_q = [1 - 10\log_{10}(\|q - q_b\|)]$ ,  $H_Q = [H_{q_1}^T, \dots, H_{q_m}^T]^T$ ,  $\Psi(q) = [\hat{\alpha}_{\text{dB}}^2 \exp(-\|q - q_1\|/\hat{\beta}), \dots, \hat{\alpha}_{\text{dB}}^2 \exp(-\|q - q_m\|/\hat{\beta})]^T$ , and  $\Phi = \Omega + \hat{\rho}_{\text{dB}}^2 I_m$  with  $[\Omega]_{i,j} = \hat{\alpha}_{\text{dB}}^2 \exp(-\|q_i - q_j\|/\hat{\beta})$ ,  $\forall i, j \in \{1, \dots, m\}$  and  $I_m$  being the identity matrix. In summary, this formulation captures the best prediction the robot can have for the channel quality at an unvisited location, based on a small number of a priori channel measurements in the same environment.<sup>4</sup> See [32] for more details and the performance of this channel predictor in different real environments.

Based on this framework, the CNR (in the linear domain) at an unvisited location  $q$ , denoted by  $\Upsilon(q)$ , can be characterized as a log-normal random variable, resulting in the following predicted required transmission power at location  $q$ ,

$$P_T(q) = \frac{(1 - 2^{\log_2 M_c})\ln(5p_{b,\text{th}})}{1.5} E\left[\frac{1}{\Upsilon(q)}\right], \quad (10)$$

where  $E[1/\Upsilon(q)]$  can be evaluated based on the log-normal distribution of  $\Upsilon(q)$ . Based on the above equation and a transmission time duration, we then predict the communication energy consumption for any unvisited location in the environment, which can then be used in the optimization of the human-robot collaboration under communication and motion energy constraints.

<sup>4</sup>The small number of prior measurements could have been obtained by the robot as it starts its operation in the environment, could have been collected in prior operations in this environment, or could have been communicated to the robot by other robots and/or through crowdsourcing.

### B. Problem Setup

Consider the setup of Fig. 1, where we have a total of  $N$  sites. In this section, we consider the case where, instead of a direct limitation on the total number of queries, the robot has a constraint on its total energy consumption, including both communication and motion energy costs. We further consider realistic communication environments, as modeled in the previous part.

Sending a query to the human operator and moving closer to a site for better sensing will incur communication and motion energy costs, respectively. The robot is then given a total energy budget  $\mathcal{E}$ , which can be used towards communication or motion for site visiting. For the  $i^{\text{th}}$  site,  $i \in \{1, \dots, N\}$ ,  $x_i$  is the deviation distance from the path. We denote the communication energy cost after deviating  $x_i$  towards site  $i$  by  $\mathcal{E}_{C,i}(x_i)$  (i.e., the cost of communicating to the operator from a location that is  $x_i$  off the main path towards site  $i$ ), while  $\mathcal{E}_{M,i}(x_i)$  denotes the motion energy cost of deviating a distance of  $x_i$ . The probabilities of correct target classification of the  $i^{\text{th}}$  site, based on the sensing performed after deviating  $x_i$  towards site  $i$ , are denoted by  $p_{r,i}(x_i)$  and  $p_{h,i}(x_i)$  for the robot and the human, respectively. In order to maximize the average correct classification probability, the robot needs to decide how far it should deviate from the main path to sense each site, and whether it should ask for help for each site by communicating to the operator after deviating  $x_i$  from the main path, subject to a total energy budget. In addition to predicting the human and robot correct classification probabilities, as we discussed in Sec. IV, the robot further probabilistically predicts its communication energy cost, using the formulation of Sec. V-A, which is needed for a proper optimization.

Similar to in Sec. IV, it is possible to formulate this optimization problem as an ILP by discretizing the continuous motion decision space, as follows:

$$\begin{aligned}\max_{\gamma} \quad & \frac{1}{N} \sum_{i=1}^N \sum_{j=1}^{D_i} \gamma_{h,i,j} p_{h,i,j} + \gamma_{r,i,j} p_{r,i,j} \\ \text{s.t.} \quad & \sum_{j=1}^{D_i} \gamma_{h,i,j} + \gamma_{r,i,j} = 1, \quad \forall i \in \{1, \dots, N\}, \\ & \sum_{i=1}^N \sum_{j=1}^{D_i} \gamma_{h,i,j} \mathcal{E}_{C,i,j} + (\gamma_{r,i,j} + \gamma_{h,i,j}) \mathcal{E}_{M,i,j} \leq \mathcal{E}, \\ & \gamma \in \{0, 1\}^{2 \times \sum_{i=1}^N D_i},\end{aligned}\quad (11)$$

where  $N$  is the number of sites and  $D_i$  is the number of motion decisions of site  $i$ . For site  $i$ , the set of decision variables is  $\{\gamma_{r,i,1}, \gamma_{h,i,1}, \dots, \gamma_{r,i,D_i}, \gamma_{h,i,D_i}\}$ , where  $\gamma_{r,i,j} = 1$  if the robot deviates  $x_{i,j}$  from the path and relies on itself for classification, while  $\gamma_{r,i,j} = 0$  denotes otherwise. Similarly,  $\gamma_{h,i,j} = 1$  if the robot deviates  $x_{i,j}$  from the path and queries the human after further sensing, and  $\gamma_{h,i,j} = 0$  denotes otherwise.  $\gamma$  is then the stacked vector of all the decision variables for all the sites, as given by Eq. (4).  $p_{h,i,j}$ ,  $p_{r,i,j}$ ,  $\mathcal{E}_{C,i,j}$ , and  $\mathcal{E}_{M,i,j}$  are nonnegative constants representing the probability of human correct classification, the probability of robot correct classification, the communication energy cost of querying the operator, and the motion energy cost, respectively, after deviating  $x_{i,j}$  for site  $i$ .

As can be seen, the energy-constrained collaborative human-

robot site surveillance problem (11) is an MCKP, a special form of MMKP, when there is only one type of resource constraint. Due to the prevalence of MCKP problems in computer science, there exists a rich body of literature for mathematically characterizing MCKPs, which we tap into next for deriving an efficient near-optimal solution to our collaborative problem.

### C. Near-Optimal LP-based Solution

As MCKP is NP-hard and computationally expensive, we show how to utilize an LP relaxation to obtain an efficient near-optimal solution to the MCKP problem (11).

Similar to Sec. IV-C, the LP relaxation is obtained by replacing the binary constraint  $\gamma \in \{0, 1\}^{2 \times \sum_{i=1}^N D_i}$  in problem (11) with a linear constraint  $\mathbf{0} \preceq \gamma \preceq \mathbf{1}$ . The following proposition describes the number of fractional variables in an optimal solution to the LP, which then allows us to relate the LP optimal solution to problem (11).

**Proposition 7.** *An optimal solution  $\gamma^*$  to the LP relaxation of the MCKP problem (11) satisfies the following:*

- 1)  $\gamma^*$  has at most two fractional variables;
- 2) If  $\gamma^*$  has two fractional variables, then they must be associated with the same site;
- 3) If  $\gamma^*$  has no fractional variables, then the solution is also an optimal solution to the MCKP problem (11).

*Proof.* The proof is similar to that of Prop. 3. Alternatively, see the proof of Prop. 2 in [35], which is a different approach based on explicitly constructing the optimal LP solution.<sup>5</sup>  $\square$

As a consequence of Prop. 7, we have the following theorem regarding the optimality gap between the optimum of the MCKP and an LP-based feasible solution.

**Theorem 2.** *Based on the optimal solution to the LP relaxation, a feasible solution can be constructed to problem (11), which is less than or equal to  $(p_{\max} - p_{\min})/N$  from the optimum of problem (11), where  $p_{\max} = \max\{p_{h,i}(x_i), p_{r,i}(x_i)\}$ ,  $p_{\min} = \min\{p_{h,i}(x_i), p_{r,i}(x_i)\}$ ,  $\forall i \in \{1, \dots, N\}$  and  $x_i \in [0, d_i]$ .*

*Proof.* The proof is similar to the proof of Theorem 1.  $\square$

Alg. 2 next describes our method of rounding the fractional variables in the optimal LP solution, which is similar to Alg. 1 in that while solving for the best binary decisions, Alg. 2 keeps the energy consumption per site the same as in the LP solution. We refer to the feasible solution to problem (11), provided by Alg. 2, as the *LP-based solution* for the rest of this section. Similar to Alg. 1, we denote  $\gamma_{\text{LP}}^*$  as the optimal solution to the LP relaxation of problem (11) and  $\gamma_{\text{LP-based}}$  as the LP-based solution to problem (11) given by Alg. 2. In the LP optimal solution  $\gamma_{\text{LP}}^*$ ,  $S_f$  is the set of sites with fractional variables and  $\mathcal{E}_i$  is the energy allocated to site  $i$  in the LP optimal solution:  $\sum_{j=1}^{D_i} \gamma_{\text{LP},h,i,j}^* \mathcal{E}_{C,i,j} + (\gamma_{\text{LP},r,i,j}^* + \gamma_{\text{LP},h,i,j}^*) \mathcal{E}_{M,i,j}$ .

### D. Properties of the Optimal Solution

Next, we study some properties of the optimal decisions.

**Proposition 8.** *In an optimal solution to problem (11), if  $\gamma_{r,i_1,j_1}^* = 1$  and  $\gamma_{r,i_2,j_2}^* = 1$ , where  $i_1, i_2 = 1, \dots, N$ ,*

<sup>5</sup>Note that we can not use the proof of [35] for the MMKP case of Sec. IV as it was developed specifically for the case of one resource constraint (MCKP).

---

### Algorithm 2: LP-based Solution to the MCKP Problem (11)

---

**CASE 1** ( $|S_f| = 0$ ): Set  $\gamma_{\text{LP-based}} = \gamma_{\text{LP}}^*$ .

**CASE 2** ( $|S_f| = 1$ ): Suppose that site  $i$  has fractional variables.

Set  $j_r^* = \text{argmax}\{p_{r,i,j} : \mathcal{E}_{M,i,j} \leq \mathcal{E}_i\}$ .

Set  $j_h^* = \text{argmax}\{p_{h,i,j} : \mathcal{E}_{M,i,j} + \mathcal{E}_{C,i,j} \leq \mathcal{E}_i\}$ .

**if**  $p_{r,i,j_r^*} \geq p_{h,i,j_h^*}$  **then**

| Set  $\gamma_{\text{LP-based},r,i,j_r^*} = 1$ .

**else**

| Set  $\gamma_{\text{LP-based},h,i,j_h^*} = 1$ .

**end**

Set the other variables associated with site  $i$  to 0. For the remaining sites, set the variables in  $\gamma_{\text{LP-based}}$  equal to the corresponding ones in  $\gamma_{\text{LP}}^*$ .

---

$j_1 \in \{1, \dots, D_{i_1}\}$ ,  $j_2 \in \{1, \dots, D_{i_2}\}$ , and  $\max\{x_{i_1,j_1}, x_{i_2,j_2}\} < \min\{d_{i_1}, d_{i_2}\}$ , then  $p_{r,i_1,j_1} - p_{r,i_1,j_2} \geq p_{r,i_2,j_1} - p_{r,i_2,j_2}$ .

*Proof.* The proof is through contradiction, similar to the proof of Prop. 5.  $\square$

This proposition says that if we have two sites  $i_1$  and  $i_2$  for which the robot relies on its own decision after deviating two different distances towards the sites,  $x_1$  and  $x_2$  respectively, then the performance gain by moving from  $x_2$  to  $x_1$  at site  $i_1$  should be greater than that at site  $i_2$ .

**Proposition 9.** *Consider a simplified scenario where*

1) *The distance between the pre-defined path and each site is the same:  $d_i = d$ ,  $\forall i \in \{1, \dots, N\}$ , where  $d > 0$  is a constant;*

2)  *$p_{r,i}(\cdot)$  is the same for all the sites. Similarly,  $p_{h,i}(\cdot)$  is the same for all the sites;*

3) *The required communication energy is constant in the vicinity of a site (does not change along the route to a site):  $\mathcal{E}_{C,i} = \mathcal{E}_{C,i,1} = \dots = \mathcal{E}_{C,i,D_i}$ ,  $\forall i = 1, \dots, N$ ;*

4) *In the route to a site, human and/or robot performance strictly increases as the sensing distance decreases.*

*Then, in an optimal solution to problem (11), if  $\gamma_{h,i_1,j_1}^* = 1$  and  $\gamma_{r,i_2,j_2}^* = 1$ , where  $i_1, i_2 = 1, \dots, N$ ,  $j_1 \in \{1, \dots, D_{i_1}\}$ ,  $j_2 \in \{1, \dots, D_{i_2}\}$ , and  $\max\{x_{i_1,j_1}, x_{i_2,j_2}\} < \min\{d_{i_1}, d_{i_2}\}$ , then  $\mathcal{E}_{C,i_1} - \mathcal{E}_{M,\delta} < \mathcal{E}_{C,i_2}$ , where  $\mathcal{E}_{M,\delta}$  is the motion energy required to move one step closer to a site.*

*Proof.* Suppose that in an optimal solution,  $\gamma_{h,i_1,j_1}^* = 1$ ,  $\gamma_{r,i_2,j_2}^* = 1$ , and  $\mathcal{E}_{C,i_1} - \mathcal{E}_{M,\delta} \geq \mathcal{E}_{C,i_2}$ . Then by letting  $\gamma_{h,i_1,j_1} = 0$ ,  $\gamma_{r,i_1,j_2} = 1$ ,  $\gamma_{h,i_2,j_1} = 1$ , and  $\gamma_{r,i_2,j_2} = 0$ , we would obtain the same objective function value with an energy saving of  $\mathcal{E}_{C,i_1} - \mathcal{E}_{C,i_2} \geq \mathcal{E}_{M,\delta}$ . The robot may then utilize this energy to move one step closer towards any site, resulting in a strictly better solution, which is a contradiction.  $\square$

Consider the case that the discretized motion step is small and thus, the energy cost for moving one step is negligible. Prop. 9 then says that, under the conditions in Prop. 9, the robot will select the sites with the best communication qualities to query the human operator, as expected.

The following proposition characterizes the optimal solution to the LP relaxation of problem (11), where we suppress the subscripts “h” and “r” in the variables as the result does not distinguish between the two cases. More specifically, given a decision variable  $\gamma_{i,q}$  for site  $i$ , where  $q \in \{1, \dots, 2 \times D_i\}$ , it can either represent  $\gamma_{h,i,j}$  or  $\gamma_{r,i,j}$ , where  $j \in \{1, \dots, D_i\}$ . We denote the corresponding human/robot performance and the energy cost of  $\gamma_{i,q}$  by  $p_{i,q}$  and  $\mathcal{E}_{i,q}$ , respectively.

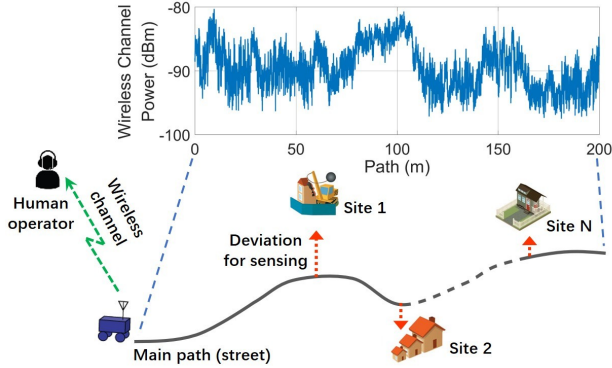


Fig. 6: The robot travels along a pre-defined main path to inspect sites near the path. Along the path, the robot's communication quality to the remote operator is subject to a space-varying wireless channel power from downtown San Francisco [46].

**Proposition 10.** For site  $i$ , if  $p_{i,j_1} \leq p_{i,j_2} \leq p_{i,j_3}$ ,  $\mathcal{E}_{i,j_1} \leq \mathcal{E}_{i,j_2} \leq \mathcal{E}_{i,j_3}$  and

$$p_{i,j_2} < \frac{\mathcal{E}_{i,j_2} - \mathcal{E}_{i,j_1}}{\mathcal{E}_{i,j_3} - \mathcal{E}_{i,j_1}} p_{i,j_3} + \frac{\mathcal{E}_{i,j_3} - \mathcal{E}_{i,j_2}}{\mathcal{E}_{i,j_3} - \mathcal{E}_{i,j_1}} p_{i,j_1}, \quad (12)$$

then in an optimal solution to the LP relaxation of problem (11),  $\gamma_{i,j_2}^* = 0$ , where  $i \in \{1, \dots, N\}$  and  $j_1, j_2, j_3 \in \{1, \dots, 2 \times D_i\}$ .

*Proof.* Suppose that in an optimal solution,  $\gamma_{i,j_2}^* = \delta > 0$ . It can be confirmed that if Eq. (12) holds, then by letting  $\gamma_{i,j_2} = 0$ ,  $\gamma_{i,j_1} = \gamma_{i,j_1}^* + \delta(\mathcal{E}_{i,j_3} - \mathcal{E}_{i,j_2})/(\mathcal{E}_{i,j_3} - \mathcal{E}_{i,j_1})$ , and  $\gamma_{i,j_3} = \gamma_{i,j_3}^* + \delta(\mathcal{E}_{i,j_2} - \mathcal{E}_{i,j_1})/(\mathcal{E}_{i,j_3} - \mathcal{E}_{i,j_1})$ , we can further improve the current optimal solution, which is a contradiction.  $\square$

Prop. 10 describes the LP-dominance property of the LP relaxation of problem (11) [35]. It says that for a site, if a decision's performance is worse than that of a certain linear combination of two other decisions, then this decision will not be selected in the optimal LP solution.

#### E. Online replanning of Communication and Motion Energy

In our proposed energy-aware collaborative planning, the robot uses its prediction of the communication energy cost for the purpose of planning, which is based on a small number of prior or online channel measurements in the same environment. As the robot spends more time in its workspace during the mission, it can collect more measurements to fine-tune the channel learning (i.e., to better predict communication energy costs). Furthermore, as the robot communicates its sensing data of a site after a site inspection, it will incur the true communication cost at that spot, which may differ from the predicted one. As such, the robot can benefit from replanning its collaborative path planning and decision making, as it obtains more channel samples and updates the cost of communication during the operation. For instance, the robot can re-solve problem (11), with the updated available energy resource, after each site visit. While re-solving the MCKP problem (11) in an online manner can be computationally expensive, especially when the problem size is large, obtaining the near-optimal LP-based solution to problem (11) is fast and efficient, allowing for online replanning, which can be key in such realistic stochastic settings.

#### F. Performance with Real Human Data and Real Wireless Channel Data

In this section, we evaluate our proposed approach using **real human data**, as described in Sec. II and also used in the evaluation part of Sec. IV. We further use **real wireless channel measurements**, which were collected along a street in downtown San Francisco [46].<sup>6</sup> This real data then presents the channel along the main path of the robot, as illustrated in Fig. 6. We assume that within the vicinity of a site, the wireless channel is approximately stationary and can be characterized by the same Gaussian random variable. Thus, the expected communication energy required to send a query near a site is constant.<sup>7</sup> There is a total of 10 sites. We assume that the sites are 10 m off the main street (main path) and 20 m apart. The robot then uses 5% a priori channel measurements to predict the channel quality in this workspace. For the communication system, 64-QAM modulation is used and the transmission time of each query is 2 s, with a target BER of  $10^{-6}$ . The receiver noise power is  $-100$  dBm. For the motion model, we have  $\kappa_1 = 7.4$ ,  $\kappa_2 = 0.29$ , and the robot travels with a constant speed of 1 m/s. The robot adopts a distance-dependent noise variance model:  $v = a_i d^2 + b_i$ , where  $a_i$  and  $b_i$  are positive constants [29]. We assume that the sites have three levels of sensing difficulty: easy, medium, and hard, encoded in  $a_i$ , which is randomly assigned to the sites. The robot then uses the proposed approach of Sec. V-B to co-plan its human collaboration and site inspection. Furthermore, after visiting each site, it learns the true channel value and the corresponding true incurred communication energy cost, and can replan its future actions over the remaining sites, using the updated true remaining energy, as discussed in Sec. V-E. Note that after measuring the channel at a site that was planned to be queried, the robot may find that the true required communication energy plus the motion energy to return to the main path will exceed its remaining budget. In this case, it will give up communication for this site and rely on its own classification instead. It then uses the remaining energy to continue replanning for the remaining sites.

**Remark 2.** (*Mission failure without replanning*) Suppose that the robot does not replan. When the robot communicates to the remote operator at a location with a worse-than-predicted channel quality, it will need to spend more energy than planned to guarantee the required end-to-end communication quality. Since the robot does not replan, it could exhaust the energy budget ( $\mathcal{E}$ ) and may not be able to arrive at the final destination eventually. Such cases are then considered mission failures. In other words, the no-replanning approach does not always provide a feasible solution, highlighting the importance of replanning.

Similar to Sec. IV-G, we compare our proposed approach with a benchmark methodology where the collaboration is not fully optimized. In this benchmark, the robot assumes

<sup>6</sup>Channel data is courtesy of W. M. Smith [46].

<sup>7</sup>We make this assumption since this real channel data from downtown San Francisco is only available along a street. As such, we assume the channel remains the same when deviating towards a site. In the next part, we show the performance in a realistic 2D wireless environment where the channel changes along a route to a site as well.

that human performance is perfect. The benchmark robot then solves problem (11) with  $p_{h,i,j} = 1, \forall i = \{1, \dots, N\}, j \in \{1, \dots, D_i\}$ .

Fig. 7 shows the average correct classification probability of our proposed LP-based solution (Alg. 2) with channel prediction and online replanning (red solid), and compares it to the benchmark with replanning (blue dashed). The performance is averaged over 100 problem instances for each given energy budget. In each instance, the 5% a priori channel measurements are randomly and uniformly chosen over the space, and each site is randomly and uniformly assigned one of the three sensing difficulty levels. The energy budget is represented as a percentage of what is needed to reach and query all the sites. The figure further shows the performance of solving the MCKP of problem (11) with perfect channel knowledge (green dashed), which provides a performance upper bound. As the figure shows, the gap between the upper bound and our approach is considerably small, even though our approach learns the channel with a small number of channel measurements (as opposed to assuming it known), and is based on solving the LP relaxation. It can also be seen that our proposed approach outperforms the benchmark significantly. For instance, given an energy budget of 0.8, the performance upper bound is 0.938, the performance of our proposed LP-based solution with replanning is 0.930, and the performance of the benchmark (with replanning) is 0.785. Note that if the robot does not replan, it may not accomplish the entire mission, as discussed in Remark 2. For instance, for the case of our proposed LP-based approach, the robot fails the operation 12.1% of the time if it does not replan, while it will fail 16.0% of the time for the benchmark case without replanning.

Table III summarizes the energy saving, enabled by our proposed approach, as compared to the benchmark. For instance, our proposed approach can achieve an average correct classification probability of 0.75, but requires 58.46% less energy consumption as compared to the benchmark. “Inf” indicates that the benchmark simply cannot achieve the specified performance no matter how much energy is given.

Fig. 8 shows a sample result using our proposed LP-based solution with online replanning. The discretized motion step is 1 m. The base station is located on the far left of the x-axis. The first and second rows show the real and the predicted channel powers along the main path, respectively. The third row then indicates the sensing difficulty associated with each site, with 0 and 2 being the easiest and the hardest, respectively. The fourth row shows the robot’s optimal deviation distance at each site. The fifth row indicates whether the robot should ask for human help at each site, with 1 indicating a query.

It can be seen that the robot queries the human operator at sites 5 and 6,<sup>8</sup> where the channel qualities are the best among all the sites. The channel power at sites 4 and 9 are also good. However, the robot does not query the human operator with these two sites. This is because the sensing difficulty is high for these two sites and the robot needs to move close to the sites for sensing, after which the robot’s own performance is already good and the improvement obtained from asking the

<sup>8</sup>The sites are indexed from 1 to 10 with the leftmost being site 1.

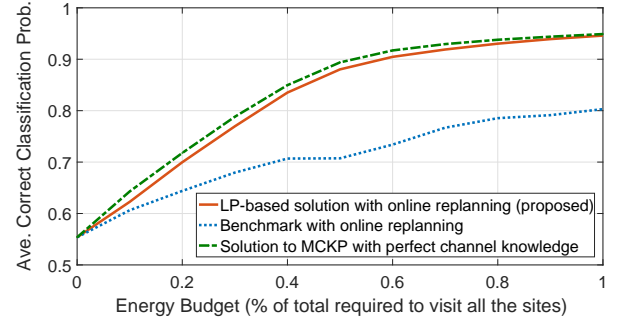


Fig. 7: The solid red curve shows the performance of our proposed LP-based solution, where the robot has a limited total combined motion and communication energy budget. The dashed blue curve shows the performance of the benchmark. The dashed green curve shows the upper bound performance of solving problem (11) with perfect channel knowledge.

Ave. Correct Classification Prob.	Percentage Energy Saving
0.60	27.78%
0.65	37.21%
0.70	46.67%
0.75	58.46%
0.80	64.80%
0.85 or higher	Inf

TABLE III: Energy saving of our proposed approach as compared to the benchmark, for the case where the robot has a limited total motion and communication energy budget.

human will be small. In other words, the robot predicts that the performance gain obtained from querying the human is better for sites 5 and 6 (as compared to sites 4 and 9), and the channel quality is also better at sites 5 and 6. For sites 2, 7, and 10, it can be seen that the robot does not deviate much from the main path for further sensing as it is easy to sense these sites. For sites with a medium sensing difficulty, the robot moves some distance towards the site locations for better sensing (sites 3, 5, 6, and 8). Among these sites, the robot deviates less at sites 5 and 6 where it queries the human. For sites that are hard to sense, the robot needs to move very close to the site locations for a reasonably good sensing quality (site 1, 4, and 9). The average correct classification probability is 0.798 in this case.

#### G. Simulation with Realistic 2D Wireless Channel

In this section, we demonstrate our proposed approach in a realistic simulated 2D wireless environment [47], where the channel parameters (obtained from real wireless measurements [32]) are  $\hat{\theta} = [-41.34, 3.86]$ ,  $\hat{\alpha}_{dB} = 3.20$ ,  $\hat{\eta} = 3.09$  m, and  $\hat{\rho}_{dB} = 1.64$ . The sensing model, motion parameters, and communication system parameters are the same as in Sec. V-F. The robot predicts the channel in this workspace based on 0.25% a priori channel samples (randomly located over the workspace), by using the framework of Sec. V-A. During the operation, the robot utilizes the LP-based approach, with online replanning when optimizing its motion and queries.

For a better illustration, we show an example result with 4 sites in Fig. 9. In terms of the sensing difficulty, site 1 is the easiest, site 2 and 4 have a medium sensing difficulty, and site 3 is the hardest to sense. The channel power (in dBm) is plotted on a 2D map with brighter colors (higher values) indicating better channel qualities. The horizontal grey

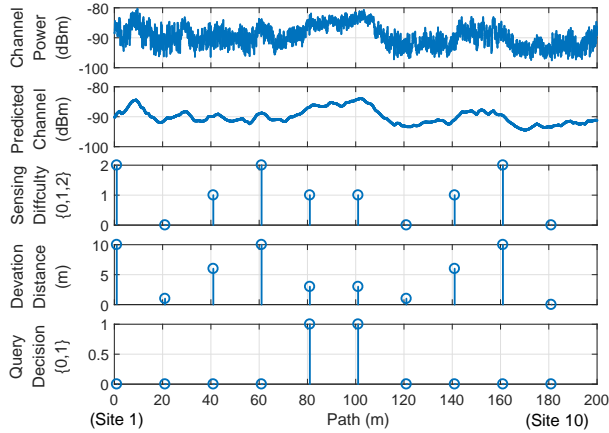


Fig. 8: The performance of our proposed energy-aware collaborative human-robot site inspection – First row: real channel power along the main path (from downtown San Francisco). Second row: predicted channel power based on 5% prior channel measurements. Third row: the height of the bars indicates the sensing difficulty level, with 0 being the easiest and 2 being the hardest. Fourth row: the height of the bars indicates how much the robot deviates from the path to sense the site. Fifth row: it shows whether the robot queries the human, with 1 indicating a query. The sites are indexed from 1 to 10 with the leftmost being site 1. The energy budget is 30% of what is needed to both reach the site locations and query the human for all the sites.

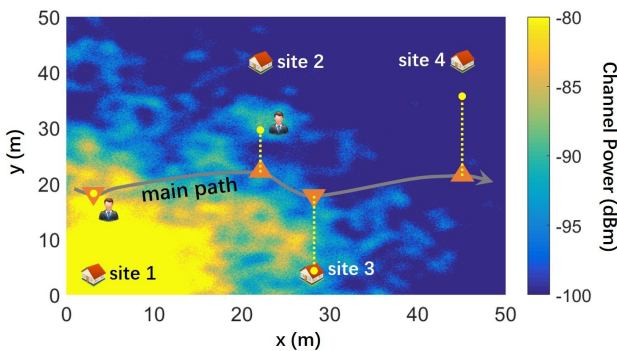


Fig. 9: Planning result in a 2D wireless environment. Brighter colors (higher values) on the channel map indicate better channel qualities.<sup>9</sup> The horizontal grey curve represents the pre-defined main path and the orange triangles are the points where the robot deviates from the main path to perform further sensing. The house icons indicate the site locations. For each site, the yellow dashed line indicates the extent of the deviation, and the presence of a human icon indicates that the robot will query the human operator. Readers are referred to the color PDF for optimal viewing.

curve represents the pre-defined main path and the orange triangles are the points where the robot deviates from the main path to perform further sensing. The house icons indicate the respective site locations. For each site, the yellow dashed line indicates the extent of the deviation and the presence of a human icon indicates that the robot will query the human operator. For each site, the terminal point of the yellow dashed line shows the location where the robot conducts further sensing and communicates to the remote operator (if the robot decides to query the operator).

<sup>9</sup>In this wireless environment, the channel power ranges from  $-5.40 \text{ dBm}$  to  $-123.06 \text{ dBm}$ . For a better visualization, we assign a light yellow color to locations with a channel power greater than  $-80 \text{ dBm}$  and a dark blue color to locations with a channel power less than  $-100 \text{ dBm}$ .

It can be seen that for site 1, the robot queries the human operator and stays on the main path. This is because site 1 is easy to sense and the required communication energy is very small for site 1, as the channel quality is very good in this region, which can be seen on the channel power map. In other words, there is no need for further sensing as both the human performance and the channel quality are already good for this site. For site 2, the robot deviates some distance and queries the human operator after sensing. In particular, the robot moves to a good channel quality region when communicating to the human, as indicated by the brighter color near the terminal point of the yellow dashed line for site 2. On the other hand, although site 4 also has a medium sensing difficulty, the robot moves much closer to the site location for sensing and does not query the human operator. This is because the channel quality near site 4 is very poor and thus, the robot has to rely on itself for classification by moving close to the site. Site 3 has a high level of sensing difficulty and the robot thus has to reach the site location for sensing. Although the channel quality near site 3 is good, there is no incentive for the robot to query the human operator as its own performance is already good after sensing at the site location. The average correct classification probability is 0.850 in this case.

## VI. CONCLUSIONS

In this paper, we studied human-robot collaborative site inspection and target classification. More specifically, we considered the realistic case where the human visual performance is not perfect, depending on the sensing quality, and the robot has constraints in communicating with the human operator. Furthermore, the robot has a limited onboard motion and communication energy budget and has to operate in realistic channel environments that experience path loss, shadowing, and multipath fading. We then showed how to co-optimize motion, sensing, and queries in human-robot collaborative site inspections under limited motion and communication resources, constraints in communication with the operator, and imperfect human visual performance. We considered two types of realistic communication constraints: 1) the robot is given a limited number of chances to query the human operator, and 2) the wireless channel quality is not good enough all over the workspace to result in a reliable communication link, necessitating the robot to optimally choose the locations for communication with the operator.

Given a probabilistic human performance characterization and a probabilistic prediction of channel quality in realistic environments, we formulated the resulting co-optimization as MMKPs. We then proposed an LP-based efficient near-optimal solution to the NP-hard MMKP, and mathematically characterized the optimality gap, showing that it can be considerably small. We also mathematically characterized several properties of the optimal solution. Finally, we validated the proposed approach comprehensively with extensive real human data, as well as with real wireless channel data from downtown San Francisco. The numerical results show that our proposed approach properly co-optimizes motion, sensing, and human queries, and can significantly outperform benchmark methodologies in terms of task performance and resource savings.

## REFERENCES

- [1] R. Olfati-Saber, A. Fax, and R. M. Murray. Consensus and cooperation in networked multi-agent systems. *Proceedings of the IEEE*, 95(1):215–233, 2007.
- [2] F. Kendoul. Survey of advances in guidance, navigation, and control of unmanned rotorcraft systems. *Journal of Field Robotics*, 29(2):315–378, 2012.
- [3] A. Krizhevsky, I. Sutskever, and G. E. Hinton. Imagenet classification with deep convolutional neural networks. In *Advances in Neural Information Processing Systems*, pages 1097–1105, 2012.
- [4] J. Kober and J. Peters. Reinforcement learning in robotics: A survey. In *Reinforcement Learning*, pages 579–610. Springer, 2012.
- [5] A. Ghaffarkhah and Y. Mostofi. Dynamic networked coverage of time-varying environments in the presence of fading communication channels. *ACM Transactions on Sensor Networks*, 10(3), 2014.
- [6] S. Branson, C. Wah, F. Schroff, B. Babenko, P. Welinder, P. Perona, and S. Belongie. Visual recognition with humans in the loop. In *Proceedings of the European Conference on Computer Vision*, pages 438–451. 2010.
- [7] A. Stewart, M. Cao, A. Nedic, D. Tomlin, and N. Leonard. Towards human–robot teams: Model-based analysis of human decision making in two-alternative choice tasks with social feedback. *Proceedings of the IEEE*, 100(3):751–775, 2012.
- [8] J. R. Peters, V. Srivastava, G. S. Taylor, A. Surana, M. P. Eckstein, and F. Bullo. Human supervisory control of robotic teams: Integrating cognitive modeling with engineering design. *IEEE Control Systems*, 35(6):57–80, 2015.
- [9] J. R. Medina, T. Lorenz, and S. Hirche. Considering human behavior uncertainty and disagreements in human–robot cooperative manipulation. In *Trends in Control and Decision-Making for Human–Robot Collaboration Systems*, pages 207–240. Springer, 2017.
- [10] X. Wang, Z. Shi, F. Zhang, and Y. Wang. Dynamic real-time scheduling for human–agent collaboration systems based on mutual trust. *Cyber-Physical Systems*, 1(2-4):76–90, 2015.
- [11] M. B. Dias, B. Kannan, B. Browning, E. Jones, B. Argall, M. F. Dias, M. Zinck, M. Veloso, and A. Stentz. Sliding autonomy for peer-to-peer human–robot teams. In *Proceedings of the International Conference on Intelligent Autonomous Systems*, pages 332–341, 2008.
- [12] S. Rosenthal, M. Veloso, and A. K. Dey. Is someone in this office available to help me? *Journal of Intelligent & Robotic Systems*, 66(1):205–221, 2012.
- [13] A. Bechar, J. Meyer, and Y. Edan. An objective function to evaluate performance of human–robot collaboration in target recognition tasks. *IEEE Transactions on Systems, Man, and Cybernetics, Part C (Applications and Reviews)*, 39(6):611–620, 2009.
- [14] Y. Chen, H. Shioi, C. Montesinos, L. Koh, S. Wich, and A. Krause. Active detection via adaptive submodularity. In *Proceedings of the International Conference on Machine Learning*, pages 55–63, 2014.
- [15] O. Russakovsky, L. Li, and Li Fei-Fei. Best of both worlds: Human–machine collaboration for object annotation. In *Proceedings of the IEEE Conference on Computer Vision and Pattern Recognition*, 2015.
- [16] D. Gurari, S. Jain, M. Betke, and K. Grauman. Pull the plug? Predicting if computers or humans should segment images. In *Proceedings of the IEEE Conference on Computer Vision and Pattern Recognition*.
- [17] M. P. Eckstein, C. K. Abbey, and F. O. Bochud. A practical guide to model observers for visual detection in synthetic and natural noisy images. *Handbook of Medical Imaging*, 1:593–628, 2000.
- [18] H. Cai and Y. Mostofi. To ask or not to ask: A foundation for the optimization of human–robot collaborations. In *Proceedings of the American Control Conference*, 2015.
- [19] H. Cai and Y. Mostofi. Asking for help with the right question by predicting human performance. In *Proceedings of Robotics: Science and Systems*, 2016.
- [20] A. Mourikis and S. Roumeliotis. Optimal sensor scheduling for resource-constrained localization of mobile robot formations. *IEEE Transactions on Robotics*, 22(5):917–931, 2006.
- [21] S. He, J. Chen, Y. Sun, D. Yau, and N. K. Yip. On optimal information capture by energy-constrained mobile sensors. *IEEE Transactions on Vehicular Technology*, 59(5):2472–2484, 2010.
- [22] T.-K. Chang and A. Mehta. Optimal scheduling for resource-constrained multirobot cooperative localization. *IEEE Robotics and Automation Letters*, 3(3):1552–1559, 2018.
- [23] Y. Mei, Y. Lu, Y. Hu, and C. Lee. Deployment of mobile robots with energy and timing constraints. *IEEE Transactions on Robotics*, 22(3):507–522, 2006.
- [24] A. Kwok and S. Martinez. Deployment algorithms for a power-constrained mobile sensor network. *International Journal of Robust and Nonlinear Control*, 20(7):745–763, 2010.
- [25] T. Setter and M. B. Egerstedt. Energy-constrained coordination of multi-robot teams. *IEEE Transactions on Control Systems Technology*, 25(4):1257–1263, 2017.
- [26] P. S. Dutta, C. V. Goldman, and N. R. Jennings. Communicating effectively in resource-constrained multi-agent systems. In *Proceedings of the International Joint Conferences on Artificial Intelligence*, 2007.
- [27] X. Ge, Q.-L. Han, and F. Yang. Event-based set-membership leader-following consensus of networked multi-agent systems subject to limited communication resources and unknown-but-bounded noise. *IEEE Transactions on Industrial Electronics*, 64(6):5045–5054, 2017.
- [28] M. Guo and M. M. Zavlanos. Multi-robot data gathering under buffer constraints and intermittent communication. *IEEE Transactions on Robotics*, 2018.
- [29] A. Ghaffarkhah and Y. Mostofi. Communication-aware motion planning in mobile networks. *IEEE Transactions on Automatic Control*, 56(10):2478–2485, October 2011.
- [30] Y. Yan and Y. Mostofi. To Go or Not to Go On Energy-Aware and Communication-Aware Robotic Operation. *IEEE Transactions on Control of Network Systems*, 1(3):218 – 231, July 2014.
- [31] U. Ali, H. Cai, Y. Mostofi, and Y. Wardi. Motion and communication co-optimization with path planning and online channel estimation. In *Proceedings of the American Control Conference*, 2016.
- [32] M. Malmirchegini and Y. Mostofi. On the spatial predictability of communication channels. *IEEE Transactions on Wireless Communications*, 11(3):964–978, March 2012.
- [33] M. Moser, D. P. Jokanovic, and N. Shiratori. An algorithm for the multi-dimensional multiple-choice knapsack problem. *IEICE Transactions on Fundamentals of Electronics, Communications and Computer Sciences*, 80(3):582–589, 1997.
- [34] H. Kellerer, U. Pferschy, and D. Pisinger. *Knapsack problems*. Springer Berlin, 2003.
- [35] D. Pisinger. A minimal algorithm for the multiple-choice knapsack problem. *European Journal of Operational Research*, 83(2):394–410, 1995.
- [36] M. S. Khan. *Quality adaptation in a multisession multimedia system: Model, algorithms, and architecture*. PhD thesis, University of Victoria, 1999.
- [37] K. Navaie and H. Yanikomeroglu. Optimal downlink resource allocation for non-real time traffic in cellular CDMA/TDMA networks. *IEEE Communications Letters*, 10(4):278–280, 2006.
- [38] J. Bellingham, M. Tillerson, A. Richards, and J. P. How. Multi-task allocation and path planning for cooperating UAVs. In *Cooperative control: models, applications and algorithms*. Springer, 2003.
- [39] M. Alighanbari and J. P. How. Decentralized task assignment for unmanned aerial vehicles. In *Proceedings of the IEEE Conference on Decision and Control*, 2005.
- [40] M. Alighanbari and J. P. How. Robust decentralized task assignment for cooperative UAVs. In *in Proceedings of the AIAA Conference on Guidance, Navigation, and Control*, 2006.
- [41] H. Oh, H. S. Shin, A. Tsourdos, B. A. White, and P. Silson. Coordinated road network search for multiple UAVs using dubins path. In *Advances in Aerospace Guidance, Navigation and Control*. Springer, 2011.
- [42] L. R. Rodrigues, J. P. P. Gomes, and J. F. L. Alcântara. Embedding remaining useful life predictions into a modified receding horizon task assignment algorithm to solve task allocation problems. *Journal of Intelligent & Robotic Systems*, 90(1-2):133–145, 2018.
- [43] S. Burer and A. N. Letchford. Non-convex mixed-integer nonlinear programming: A survey. *Surveys in Operations Research and Management Science*, 17(2):97–106, 2012.
- [44] S. Boyd and L. Vandenberghe. *Convex optimization*. Cambridge university press, 2009.
- [45] A. Goldsmith. *Wireless communications*. Cambridge university press, 2005.
- [46] W. M. Smith. *Urban propagation modeling for wireless systems*. PhD thesis, Stanford University, 2004.
- [47] A. Gonzalez-Ruiz, A. Ghaffarkhah, and Y. Mostofi. A comprehensive overview and characterization of wireless channels for networked robotic and control systems. *Journal of Robotics*, 2011.



**Hong Cai** received the B.E. degree in electronic and computer engineering from the Hong Kong University of Science and Technology, Kowloon, Hong Kong, in 2013, and the M.S. degree in electrical and computer engineering from the University of California, Santa Barbara, CA, USA, in 2015, where he is currently working toward the Ph.D. degree with the Department of Electrical and Computer Engineering.

His research interests include human-robot collaboration, learning and prediction of human performance, communication-aware robotics, and optimization of robot decision making and planning.



**Yasamin Mostofi** received the B.S. degree in electrical engineering from Sharif University of Technology, Tehran, Iran, in 1997, and the M.S. and Ph.D. degrees in the area of wireless communications from Stanford University, California, in 1999 and 2004, respectively. She is currently a professor in the Department of Electrical and Computer Engineering at the University of California Santa Barbara. Dr. Mostofi is the recipient of 2016 Antonio Ruberti Prize from IEEE Control Systems Society, the Presidential Early Career Award for Scientists and Engineers (PECASE), the National Science Foundation (NSF) CAREER award, and the IEEE 2012 Outstanding Engineer Award of Region 6, among other awards. Her research is on mobile sensor networks. Current research thrusts include communication-aware robotics, human-robot networks, RF sensing, X-ray vision for robots, see-through imaging, and occupancy estimation. Her research has appeared in several reputable news outlets such as BBC, Huffington Post, Daily Mail, Engadget, and NSF Science360. She has served on the IEEE Control Systems Society conference editorial board 2008-2013. She is currently an associate editor for the IEEE TRANSACTIONS ON CONTROL OF NETWORK SYSTEMS. She is a senior member of the IEEE.